REPUBLIC OF TÜRKİYE

ALTINBAŞ UNIVERSITY

Institute of Graduate Studies

Civil Engineering

CALCULATION AND COMPARISON OF PERIODS OF TALL STRUCTURES WITH FORCE METHOD – GROUP LOADING AND ETABS

Nimr Hatem AL-DULAIMI

Master's Thesis

Supervisor

Prof. Dr. Zeki HASGÜR

Istanbul, 2023

CALCULATION AND COMPARISON OF PERIODS OF TALL STRUCTURES WITH FORCE METHOD – GROUP LOADING AND ETABS

Nimr Hatem AL-DULAIMI

Civil Engineering

Master's Thesis

ALTINBAŞ UNIVERSITY

2023

The thesis titled CALCULATION AND COMPARISON OF PERIODS OF TALL STRUCTURES WITH FORCE METHOD – GROUP LOADING AND ETABS prepared by NIMR HATEM AL-DULAIMI and submitted on 14/04/2023 has been **accepted unanimously** for the degree of Master of Arts/MBA/Master of Science in Civil Engineering

____

Prof. Dr. Zeki HASGÜR

the Supervisor

Thesis Defense Committee Members:

Prof. Dr. Zeki HASGÜR	Department of Civil Engineering, Altınbaş University	___________________
Prof.Dr. Tuncer ÇELİK	Department of Civil Engineering, Altınbaş University	___________________
Prof. Dr. Bariş GÜNEŞ	Department of Civil Engineering, Istanbul University-Cerrahpasa	___________________

I hereby declare that this thesis meets all format and submission requirements of a Master’s thesis.

Submission date of the thesis to Institute of Graduate Studies: ___/___/___

I hereby declare that all information/data presented in this graduation project has been obtained in full accordance with academic rules and ethical conduct. I also declare all unoriginal materials and conclusions have been cited in the text and all references mentioned in the Reference List have been cited in the text, and vice versa as required by the abovementioned rules and conduct.

Nimr Hatem AL-DULAIMI

Signature

ABSTRACT

CALCULATION AND COMPARISON OF PERIODS OF TALL STRUCTURES WITH FORCE METHOD – GROUP LOADING AND ETABS

AL-DULAIMI, Nimr Hatem

M.Sc., Civil Engineering, Altınbaş University,

Supervisor: Prof. Dr. Zeki HASGÜR

Date: April / 2023

Pages: 85

In view of the huge possibility for the deployment of current reliability systems in the structures, it is imperative that the efficiency of each method be evaluated, analyzed, and demonstrated in order to persuade the firms that design buildings to adopt them. Attributed to the reason that time history impulses recorded at a specific location are the result of a random process that is nearly impossible to replicate, a substantial amount of effort has been invested in recent years into the processing of actual records in order to make them "representative" of future input histories to construction that is already in place as well as construction that is planned to be built in areas that are prone to earthquakes. In this investigation a G+20 story structure with various structural systems including moment frame, bracing system and shear wall was analyzed to find the actual structural response under the dynamic analysis. Further the brace frame and the shear wall model were analyzed according to the site dependent spectra and for this the EI-Centro earthquake data was taken for the analysis. From the analytical result both the model consists of shear-wall and bracing system depicted significant improvement in the stability and the time period of the structure in the linear dynamic analysis. While comparing the nonlinear time-history analysis against the EI-Centro earthquake data both the shear wall and brace frame model was comparable and depicted enough structural stability, however, the shear-wall depicted the over-all

performance improvement when comparing the data against the earthquake time acceleration.

Keywords: Ground Accelerations, Nonlinear Dynamic Response, Story Drift, Seismic Analysis.

TABLE OF CONTENTS

Pages

LIST OF TABLES

Pages

LIST OF FIGURES

Pages

1. INTRODUCTION

1.1 GENERAL

Seismic design of any structural systems is typically comprised the design elements that provide the greatest degrees of hazards, difficulties, as well as unpredictability towards the design. The Equivalent Static Force Procedure (ESFP) is a widely used code-based seismic design method that determines overall earthquake forces of normal structures (ESFP). Similar to any simplified techniques, The ESFP method possesses restrictions such as the evaluation of a building's fundamental period, the lack of tools to determine response metrics apart from force and displacement, the exclusion of higher modes, as well as the inability to incorporate the multi-directional characteristics of large earthquakes.

1.2 BACKGROUND OF THIS STUDY

It has become widely accepted that response spectra generated from elastic assessments of structures exposed to earthquake events frequently fail to accurately forecast overall hierarchies of fatigue damage. The energy intake as well as pressure transfer processes that arise from a building's slow plastic hinge creation are equally difficult to measure. It is essential in evaluating newly constructed or existing infrastructures having great significance such as nuclear power plants and holding tanks, uncertainty like unusual structures and coupled soil-structure processes, greater standard of inelasticity like systems intended to demonstrate crack propagation, as well as dimensional nonlinear effects like base-isolated infrastructures. Investigating the inelastic structure reaction inside this time domain is the sole way to learn such data. Whenever dominant modes of vibration are narrowly divided apart [1] or for multiple-supported infrastructures such as bridges in which higher modes can be generated [2] by the approaching seismic activity’s asynchronous character, the dynamic time history analysis as well as the linear elastic analysis is particularly helpful.

LTHA can be utilized for significantly lessening the ESFP's drawbacks as well as accompanying uncertainty. The application of time history analysis is frequently used in investigation, but technical experts have not completely embraced it as a useful analytical technique. The numerical work required to conduct analysis of time history for the infrastructure’s designing and retrofitting has already been reduced as a result of improved hardware processing capacity and the advanced computer-aided development tool’s accessibility. As a result, time history analysis may be used as an industry's main analytical technique, resulting in more effective and affordable solutions.

Because of the exponential increase throughout computing power as well as the advancement of software packages over the past years, complex structures involving numerous degrees of freedom are now subjected to elastic and inelastic dynamic assessments in the time domain. Time-domain analysis is therefore required by the maximum existing seismic provisions. In contrast, current research has demonstrated that the seismically ground motion appears to be the greatest unforeseeable event [3] and exerts a major effect upon that fluctuation seen in the structural behavior [4] across all uncertainties that are arising from the designing concept, the components characteristics such as quality of the supporting soil, steel and concrete, , as well as the seismic activity itself. Because of the natural intricacy of the pathway which prone to earthquakes produced vibrations take while these pass from the fault-plane base into substrate [5] and subsequently through the subsoil to approach its foundational layer of a building [6], ground motions really behave unpredictably in spatial and temporal.

Despite the aforementioned unpredictability, as well as the comparatively simple seismic code template considering transient dynamic assessment, it remains the designer's duty to establish a "satisfactory" method for choosing a collection of "adequate" seismic response. This work is both technologically simple as well as challenging at the same time because any imbalance inside the calculated structural behavior should be avoided as much as possible. Without a grasp of the fundamental ideas underlying both choice and sizing the seismic recordings used for dynamic analysis, it is a difficult operation which cannot be completed by using "trial and error." Additionally, the existing code guideline for seismic activity record collection has been thought to be relatively standardized considering the possible implications of the selection upon that dynamic analysis, offering the mistaken perception that structural analytical results are as reliable as the refined finite element model utilized.

Therefore, the objective of this thesis is to display a quantitative evaluation of presently offered dynamic analytical techniques to identify ground motion documentation, examine the conceptual basis of the issue as well as explore its consequences for the evaluation of large-scale structures with numerous engineering structures. In this investigation a G+20 story structure with various structural system including moment frame, bracing system and shear wall was analyzed to find the actual structural response under the dynamic analysis. Further the brace frame and the shear wall model were analyzed according to the site dependent spectra and for this the EI-Centro earthquake data was taken for the analysis. The performance of the models was analyzed under the nonlinear time history analysis. The analytical assessment also shows the variation of the time period of the same structure under the linear dynamic and non-linear dynamic analysis.

1.3 OBJECTIVES

The objectives are as follows.

a. To investigate overall response of a G+20 story structure against the dynamic analysis.

b. To examine the models according to the site dependent spectra and for this the EI-Centro earthquake data was taken for the analysis.

c. To determine the variation of the lateral response, displacements, structural integrity and time period of the same structure under the linear dynamic and non-linear dynamic analysis.

1.4 ORGANIZATION OF THE THESIS

The thesis paper contains the following chapters:

Chapter 1: Introduction

This section discusses the research significance on that investigation topic. It also includes overall purpose of the investigation as well as the outline of research.

Chapter 2: Literature Review

This section includes the background of this research. It describes the terms and conceptions related to this study briefly. It also shows the procedure how this research is important and how the research is processing.

Chapter 3: Research Methods

This section is related with the processes and consequences adopted in the research. This section also discusses about the details of methodology which have been used in this research work. This shows various properties of the materials, analysis procedures and adopted analytical method. This section shows that how the work has been done.

Chapter 4: Results and Discussion

This section shows all test findings which have been done. The necessary graphs and tables are also shown here. The explanation of these results is also described in this chapter.

Chapter 5. Conclusions and Recommendations

This section includes overall outputs, decisions, and consequences. It also includes references. This also mentions advice for further studies about the topic.

2. LITERATURE REVIEW

2.1 GENERAL

This chapter includes an evaluation of earlier work and focuses on the scope of doing new & advanced research. Typical analysis systems of moment frame, brace frame, shear walls, design procedures and analysis methods that can be utilized to design shear wall are all discussed comprehensively in this chapter.

2.2 ANALYTICAL PROCEDURES ABOUT MRF MODELS

Because of the frequent incident of rapid deterioration of beam-to-column connections, recent earthquakes around the earth (Kobe, 1995; Van, 2011) have generated several questions concerning the seismic response of moment resistant frames (MRF) [7, 8]. The impact of brittle fractures upon that earthquake capability of preexisting moment frames was reviewed in several numerical investigations [9-12]. That compelled this field of earthquake engineering to develop better structural solutions in order to prevent rapid catastrophe [13, 14].

Conversely, whenever put through many inelastic repetitions because of low cycle fatigue, new methodologies to calculate such hazard might not be unbeatable [15-20]. It's especially obvious in high-rise structures that are susceptible to long-lasting ground motions which take place close nearby the subduction zones. The principal lengths of such ground movement often last for a few minutes, whereas its prominent periods ranging from many to ten seconds [21, 22]. High-rise structures with primary natural durations greater than 2 s have a tendency to resonance with these ground vibrations. Recently available shaking table studies which simulated typical Japanese high-rise construction supported that finding [23]. At EDefense, the world's biggest shaking table center, several experiments were carried out. This resonance curves brought on by ground motion is shown in Figure 1. That very same finding was also supported by earlier computational research [24] involving tall structures exposed to lengthy ground vibrations.

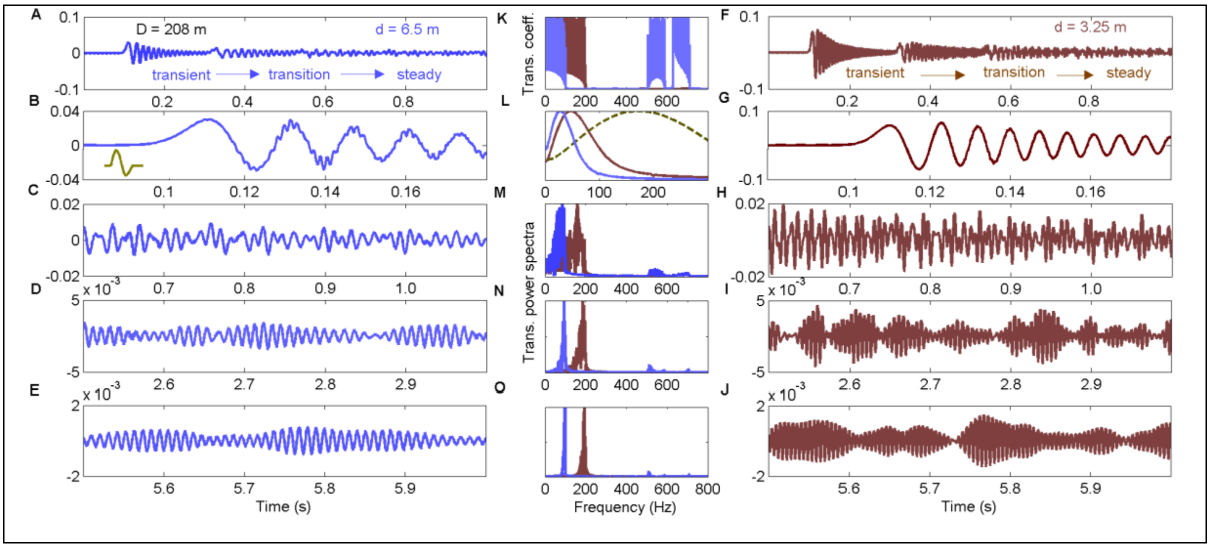

Figure 2.1: Resonance Effect Due to Ground Motion.

Numerous experiments and numerical investigations have focused on the effect of crack upon that MRF's earthquake endurance over the previous several decades as a result of earthquake loads. The impact of moment redistribution brought about by beams crack in metal MRF depending upon static loading was examined by Nakashima et al. [25] The major finding of this research was that whenever twists related to crack is relatively significant, consecutive cracks become less probable to occur throughout static moment redistribution. As a component of a SAC phase II project undertaken in the United States, making extensive use of MRFs.

Luco and Cornell [9] evaluated the impact of connections brittle cracks upon earthquake drifting needs of metal MRFs by implementing a numerical analytical model. They came up with the conclusion that at larger drift requirement levels, the impacts of shear crack are much more noticeable.

2.3 PREVIOUS ANALYTICAL ASSESSMENTS OF BRACED FRAME STRUCTURES

Correctly predicting seismic vulnerability as well as the corresponding pressures on the infrastructures is one of the key aspects of building earthquake assessment. Relatively close field seismic features must be present in seismic events that are thought to have occurred nearby faults. One of most significant characteristics include fling and forward directivity influences, that generate a powerful pulse or perhaps a string of beats with a lengthy time.

In steel frames featuring V-shaped braces both near- and far-fault seismic, Abdollahzadeh et al. [26] evaluate hysteretic energy as well as inter-story drifting. Based on the findings, evenly distributed near-fault data are more important regarding inter-story drift than far-fault recordings. Additionally, they found that the near-fault recordings contribute more to hysteretic energy compared to the far-fault records.

Wen et al. [27] investigated the influence of the location on the seismic susceptibility of high-rise shear wall structures. The findings demonstrate that because of the larger low-frequency, far-field seismic causes more significant damage to high-rise buildings than near-field earthquake. Thus, high-rise structures above soft ground that are vulnerable to far-field seismic events suffer greater losses compared to those on bedrock sites that are vulnerable to near-field seismic events.

The impact of near-field seismic events upon this performance of moment-resisting frameworks are assessed by Sharif and Behnamfar [28]. Findings suggest that the reaction is highly dependent on the proportion of the building's fundamental frequencies to the pulse's regulating duration, which can sometimes lead to a building's pressure demanding proportions growing or even transferring to higher storeys.

The consequences of fling phase and forward directivity upon that seismic behavior of structures were investigated by Kalkan and Kunnath [29]. The greatest demand for pulse-type input relies on the relationship between the building's fundamental period and the pulse period. It was discovered that recordings containing fling impacts largely excited components within their natural frequencies, whereas waves including forward directivity in the lack of fling engaged higher modes. It is determined that when taken together, the speed and velocity spectrum can be used to accurately gauge the damage potential of near-fault recordings.

Alonso-Rodrı´guez and Miranda [30] investigated the structural performance under near-fault ground vibrations by employing streamlined modeling. By conducting a number of test statistics, this was discovered that the primary important factor affecting flooring speed as well as inter-story drift requirements whenever near-fault pulse-like ground motion happens is time period.

The nonlinear behavior of tall structures under pulse-type intense ground vibrations was researched by Tehranizadeh and Meshkat-Dini [31]. As per the nonlinear studies, a structure's maximal structurally need is determined by the proportion of its pulse period towards its fundamental period.

Nevertheless, it was not until after the Northridge earthquake of 1994 that the conclusions of such research [32-34], became significantly important in practical application. As a result, the Northridge earthquake in 1994 primarily caused bracing fracture-related losses to steel-braced structures. For illustration, harm to one of the conventional steel-braced structures near Lankershim Boulevard, 17 km to the east-southeast of the core of the Northridge earthquake, is shown in [35] as a classic example of these casualties. Six bays featuring chevron framing installed within every orientation were used to withstand severe earthquake stresses inside the four-story corporate structure, which was built in accordance with the 1980 Los Angeles Building Code [36]. According to the inspection report published [35], all six N-S-oriented bays of the thin-walled second story braces collapsed during seismic.

As it was previously indicated, seismic pressures must be characterized during the building designing process either through a homogeneous response spectrum or through documented velocity time patterns providing inputs to a dynamic analysis. Another scenario requires that input motions be chosen to reflect local seismic events while also being consistent with anticipated (as well as planned) seismic events. Therefore, to employ genuine data within the context of transient dynamic assessment, they must satisfy expected seismic circumstances. The assessment of certain critical aspects of significant ground movement anticipated to take place throughout a specified time frame at a chosen area is connected to the (SHA), that has been the subject of numerous studies that provide ways to identify seismic possibilities [37].

The deterministic and probabilistic techniques are the two primary techniques for SHA. Strong-motion parameters are determined inside the (DSHA) for the highest seismic events, that is supposed to happen just at nearest available distance from location, taking into account the seismotectonic characteristics of the nearby region as well as all statistical evidence on previous earthquakes from this geographical area [38, 39]. The DSHA findings that may be employed towards document choosing are the intensity as well as distance pair which leads to he maximum ground movement magnitude at the area of interest. On the contrary, the formulation of the designing seismic situation is no simpler whenever PSHA is used to predict seismic pressures. To offer any prediction of strong-motion characteristics with a specified probability value, PSHA specifically performs an integration over the forecasting seismic events within a certain period of exposure [40-42]. A location specified homogeneous hazards reaction spectrum which is utilized for generating spectral compatibility with the pre-selected data can be produced through using PSHA to create hazardous contours, and graphs of spectral acceleration across different implementation times [43]. However, a PSHA obscures overall strong relevance of a seismic in terms of magnitude, source-to-site distances, and ground shaking divergence (e). Finding a sample seismic event that is consistent with the PSHA approach's outcomes is preferable in order to facilitate the practical assessment of the findings and to allow for engineering-type judgments [44]. The calculated probable magnitude of an earthquake can be de-aggregated (or disaggregated) to accomplish this [45, 46]. This approach can therefore be used to specify the M-R-e groups which represent the most frequent seismic events at a chosen area.

2.4 PREVIOUS ANALYTICAL ASSESSMENTS ABOUT SHEAR WALL

The aim of seismic analysis is to maximize overall structural frameworks' capability during ground movement by Moment Frames [47-50], Shear-Walls [51, 52], and Braced Frames. As prediction of collapse during seismic loading has been an important component of structural engineering, experts may utilize this collapsing probability as a critical decision criteria when designing new infrastructures as well as assessing the earthquake resistance capacity of existing structures during earthquakes [53]. According to earlier research, the higher portions of the structures are the most important since they are impacted by both subsoil stiffness as well as structural vibrations [50, 54-57]. Therefore, a variety of analysis methods are employed to anticipate the destruction resulting from ground movement, including the overall infrastructure simplification to a similar single-degree-of-freedom method [58-61], the application of processive finite-element evaluation of the entire system to diagnose an enormous change in structural behaviour [60, 61] as well as suddenly established accumulative dynamic analysis [62-65]. With regard to the RC structure, the response spectrum technique particularly permits to use the response spectrum, which is characterized as a realistic illustration of peak response vs normal time for a particular accelerogram. Dynamic analysis must be performed to determine the maximum responsiveness to a baseline stimulation for a structure and also to examine its characteristics throughout ground movement [66].

Assuring that structures meet specific quality standards (such as minimal damage, considerable harm, and collapse mitigation) while subjected to a seismic attack is a crucial aspect of high-rise building designs. Different earthquake design and assessment methodologies were created to overcome this problem. It is hard to foresee the magnitude and timing of upcoming disasters, despite seismology's ongoing advancements. The use of probabilistic approaches in the evaluation and planning procedure is essential because of the earthquake's unpredictable character. One of these statistical models is performance assessment through dynamic analysis including fragility assessment, that demonstrates the best structural functionality during earthquake loading in addition to the probability of going above a specific damage level. That style of dynamic analysis has been utilized to assess the earthquake vulnerability of structures composed of various building materials. Because of the perceived significance attached to this type of structure, numerous investigators who implemented similar approach to high-rise RC structures concentrated on those with more than 30 floors. To illustrate, Applying linear dynamic simulation with nonlinear time history assessment, Ji et al. [67] established the analytical behavior of a 54-story RC structure. Alwaeli, et al. [68] used incremental dynamic analysis (IDA) to produce fragility curves for a30-storied RC structural model. Değer, et al. [69]; Değer and Wallace [70] investigated the seismic behavior of a 42-storied reinforced concrete structure with several structural components, comprising core wall buildings equipped with and without MRF as well as a duel-system developed utilizing two separate methodologies. Employing IDA tools, Aman, et al. [71] evaluated the comparative earthquake effectiveness of five 60-storied reinforced concrete structures of various concrete strengths. It was determined that high-strength concrete not only reduces building costs but also behave seismically more safely than conventional concrete strength at higher ground movement intensity ranges. Despite the fact that mid- to tall structures are crucial to research, their prevalence is typically smaller than that of regular structures, which are frequently utilized like homes. There is a critical necessity to investigate the earthquake resistance of lower high-rise structures employing dynamic analysis since the collapse and fall of these high-rise structures will have an immediate effect on the lives of millions of occupants.

There are numerous academic papers regarding shear wall structures' earthquake sensitivity. However, only few of them covered the connection among shear wall designs and earthquake behavior of structures. In order to evaluate actual optimum top story deformations, Firoozabad, et al. [72] performed a linear time history study using structures containing six different shear wall layouts that had been subjected to two actual seismic events. It was discovered that stronger seismic activity would not necessarily result from larger shear barriers. Chandiwala [73] compared the base shear pressures of the five shear wall places within an identical L-shaped high-rise (random arrangement in plan) and came to the conclusion that for L-shaped construction drawings, the shear wall at the extreme ended up giving the greatest result through immediately impeding terminal oscillation throughout earthquakes as well as lowering bending moment of the high-rise. Sardar and Karadi [74] analyzed the ELF and response spectrum of five 25-story structures having identical layout and five different shear walls arrangements. Structures with L-shaped shear walls around extremities including core shear walls produced minimal base shear, as shown by evaluating respective story shear forces, drifts, as well as shear deformations. Three high-rise RC buildings with varying numbers of shear walls and an identical Y-shaped structure were constructed and assessed by Kim, et al. [75]. The structure with the greatest number of shear walls seemed to have the greatest strength and offered the greatest spatial variability freedom, even though additional resources were needed, according to the IDA and nonlinear static pushover analysis.

2.5 BEHAVIOR OF HIGH-RISE STRUCTURES

Knowing and accurately assessing the behavior of tall structures is essential to construct analytical models that can adequately represent such specific structures. Skyscrapers are basically vertical cantilevers that try to be loaded axially from gravity and horizontally from winds and earthquakes..

Transferring live and dead weights to and from the foundation via structures is generally not considered a difficult problem. However, load flow and additional shear forces, moments, and bending in structures that receive horizontal loads may require more complex calculations than the first-order response that can be reliably used in vertical load calculations. Often, the main cause of this complexity is the behavior of the structure and the assumptions made in the model representation of the actual structure. A satisfactory model should behave like a structure or prototype under lateral loads.

The resistance of the structure against moments is provided by the response of vertical members to bending or axial movement. The ratio of the sharing between the axial movement and bending behavior of the vertical elements due to the moments is related to the shear stiffness of the elements connecting the vertical elements. The use of more rigid fasteners contributes to a more rigid and more effective structural behavior by providing a greater amount of axial loads to be carried on the vertical elements. In this context, the design of floors, tie beams, floor diaphragms and braces that provide the connection between the vertical elements in the building is important.

Resistance to horizontal shear forces acting on the floor of tall structures is provided by the horizontal components of vertical bar shear and traverse shear. The structural members, which make the connections between the vertical members mentioned in the previous paragraph, distribute the moments as shear forces to the vertical members.

The bending of the building can vary mainly due to the horizontal component of the axial force of each diagonal reinforcement due to the irregularity of the vertical members, mass distribution problems and irregularities from elevators, stairs and auxiliary shafts. If the bearing elements and shafts to which the torsional stiffness is assigned are designed and modeled correctly, the torsional stiffness of the structure will also be shown correctly.

Structural analysis aims to realistically represent the behavior of structures under vertical and seismic loads. This process can be divided into three phases: modelling, analysis and evaluation. The modeling stage is the most important stage and affects other stages as well. Different models can be proposed according to different assumptions. Various assumptions need to be made to predict the response of a structure. These assumptions vary for reasons such as computer technology development, time management, and program modeling capabilities. An important point in the modeling phase, which is one of the most important stages of structural analysis, is to remember that, according to Powell (2010), the structural analysis model does not have to be a precise and complete model, and there will never be such a model. The use of non-linear time history analysis results when evaluating the performance of skyscrapers is currently considered the most reliable method.

To understand the reasons and reliability of using this method, we first need some considerations of high-rise behavior and a summary of the above classical analytical methods. The assumption that the structure remains fully elastic during strong seismic ground motions cannot satisfy the designer as inelastic deformation occurs beyond the limits. In classical methods, while performing force-based design, linear elastic responses are reduced by an “R” response coefficient, which depends on the structural system and ductility of the structure, and inelastic responses are indirectly taken into account. By directly considering the inelastic behavior of nonlinear structures, time domain analysis provides the opportunity to interpret the behavior of structures after different damage limits for different earthquake probabilities. Unlike conventional linear elastic methods, nonlinear time history analysis explicitly takes nonlinear behavior into account and, when designed accordingly, gives very reasonable results under maximum seismic loads (Moehle 2005).

2.6 INVESTIGATIONS ABOUT SITE DEPENDENT SPECTRA

Investigating local seismotectonic characteristics and how significantly they influence overall ground motions observed throughout an earthquake tremor is a significant topic of research. Ground movements produced via submerged rupture-type seismic events inside the time interval approximately 1.0 s are much higher than ground movement produced via ground rupture occurrences, according to Kawaga et al. [76]. Campbell [77] had shown a few discrepancies in the expected output spectra obtained from powerful movements in shallow stable regions (Europe, Eastern USA), which are shallow, whereas Bolt and Abrahamson [78] along with Lin and Lee [79]] illustrated that maximum ground motions from subduction zone seismic events typically deaden more gradually than those caused by shallow crust seismic events in geologically active areas. Additionally, Kappos et al. [80, 81] examined the elastic and inelastic spectra regarding structural stability as well as deformations in order to investigate the impact of various seismotectonic settings on seismic powerful movements. Furthermore, data derived from the NGA program's calculations [82] showed that seismic activity involving reverse-oblique mechanisms share features with reversal criticizing occurrences.

Stafford et al. [83] found no considerable variation among ground movement throughout western North America vs those within Europe and the Middle East after examining the degree toward which major ground motion prediction formulas from of the NGA might be implemented to earthquake risk evaluations throughout Europe and the Middle East. It follows logically that it may be advantageous to amalgamate these two data in order to expand the total number of records which are accessible for dynamic analyses.

3. METHODOLOGY

3.1 VARIOUS STRUCTURAL IRREGULARITIES AND THEIR LIMITS

3.1.1 Story Stiffness

When an earthquake strikes, the points of weakness in a structure are the first to give way. This fragility results from a break in the consistency of the structure's mass, stiffness, and shape. Structures that have breaks in their continuity are referred to as having an irregular shape.

3.1.2 Horizontal Irregularity (Soft Story)

It is present if the stiffness of a floor is less than 70 % also, it is present if the above three floor stiffness is gained not more than 80%.

3.1.3 Horizontal Irregularity (Extreme Soft Story)

To meet the criteria for its existence, a story's lateral stiffness must be either below 60% compared to the level beneath as well as 70% less than both the mean stiffness.

3.1.4 Weight (Mass) Irregularity

It is said to be present in a location in case the effective weight of one story is greater than 150 percent of the effective index of one of the stories that is adjacent to it. It is not necessary to take into consideration a roof that is thinner than the floor that is below it.

3.1.5 Story Displacement

Under strength-level design earthquake stresses, the seismic displacement is the actual horizontal deformation of any location in the structure relative to its base. Figure 3.1 represents an illustration of story displacement.

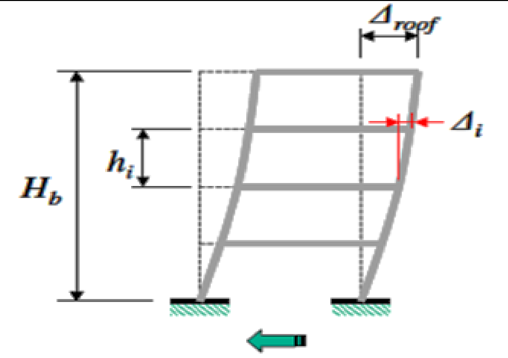

Figure 3.1: Story Displacement.

3.1.6 Drift

The lateral displacement of a floor in relation to the floor below is referred to as story drift, and the story drift ratio is calculated by dividing the amount of story drift by the total height of the building. Figure 3.2 represents an illustration of story drift.

Figure 3.2 demonstrates how to compute the "story drift," which is defined as the "relative elastic displacement" of one narrative in relation to the tale below it. On the other hand, the points awarded for this comparison will change depending on the following:

a. For a structure in which the centers of mass are aligned, the narrative drift can be estimated by looking at the deformations of the cores of mass.

b. It is possible to calculate the drift of a building in which the centers of mass are not aligned by making a vertical prediction of the mass center of the upper story to the core of mass of the lower story, and then using the deflection of the projected point.

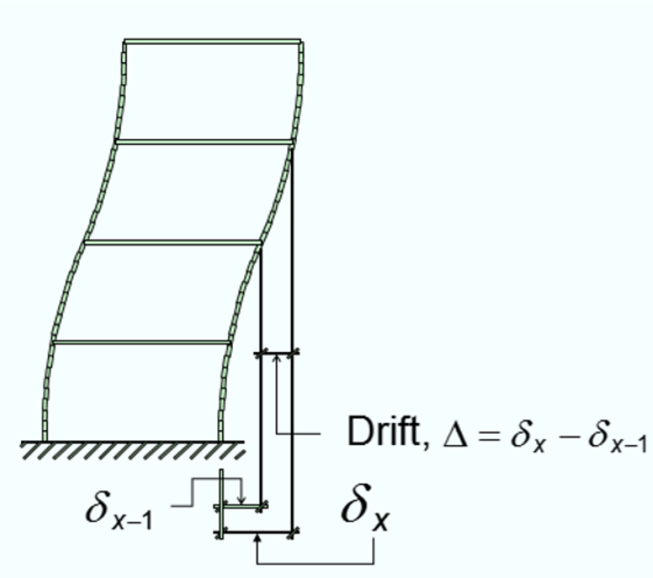

Figure 3.2: Story Drift.

The Design Δ, drift, denoted by the symbol, is determined by subtracting the Design Seismic Deflections, denoted by the symbol δ_D, at the centers of mass situated at the top or bottom of the stories that is being taken into account. It is permissible to calculate the displacement at the bottom of the tale depending on the vertical projection of the mass's center at the top of the story in cases when the centers of mass do not line vertically.

When calculating the design story drift, it is possible to ignore the effects of diaphragm deformation. The rotation of the diaphragm is to be considered in the following manner. For buildings that are classified as Seismic Category C, D, E, or F and feature horizontal irregularity, the design story drift, denoted by the symbol, must be calculated using the biggest difference between the design earthquake and the actual earthquake. repositioning of collinear points located at the top and bottom of the Δ under examination along any of the sides of the building, taking into account the consequences of diaphragm rotation. Table 3.1 outlines the allowable amount of story drift in accordance with ASCE 7-22.

Table 3.1: Allowable Story Drifts.

Structure type	Risk Category		
	I or II	**III**	**IV**
Structures that are not masonry shear wall structures and that are fewer than four stories above the foundation and have internal walls, divisions, and ceilings that have been constructed to accommodate the drift associated with the Design Earthquake Displacements are considered to be seismically resistant.	0.025h	0.020h	0.015h
Structures made of masonry with cantilever shear walls	0.010h	0.010h	0.010h
Other constructions that use masonry shear walls	0.007h	0.007h	0.007h
Every other type of buildings	0.020h	0.015h	0.010h

3.1.7 Base Shear

Base shear is an estimate of the largest predicted lateral force acting on the base of the structure as a result of seismic activity. This force acts laterally and causes the structure to move laterally. For the purpose of computing it, the seismic zone, the soil material, and the equations for lateral force taken from the building code are utilized (Figure 3.3)

The base shear of a structure, denoted by V, in a certain direction needs to be computed using the following equation:

$$V = C_s W \tag{3.1}$$

Here, Response coefficient, denoted by the symbol Cs,

W = The Actual Seismic Weight for Each Section

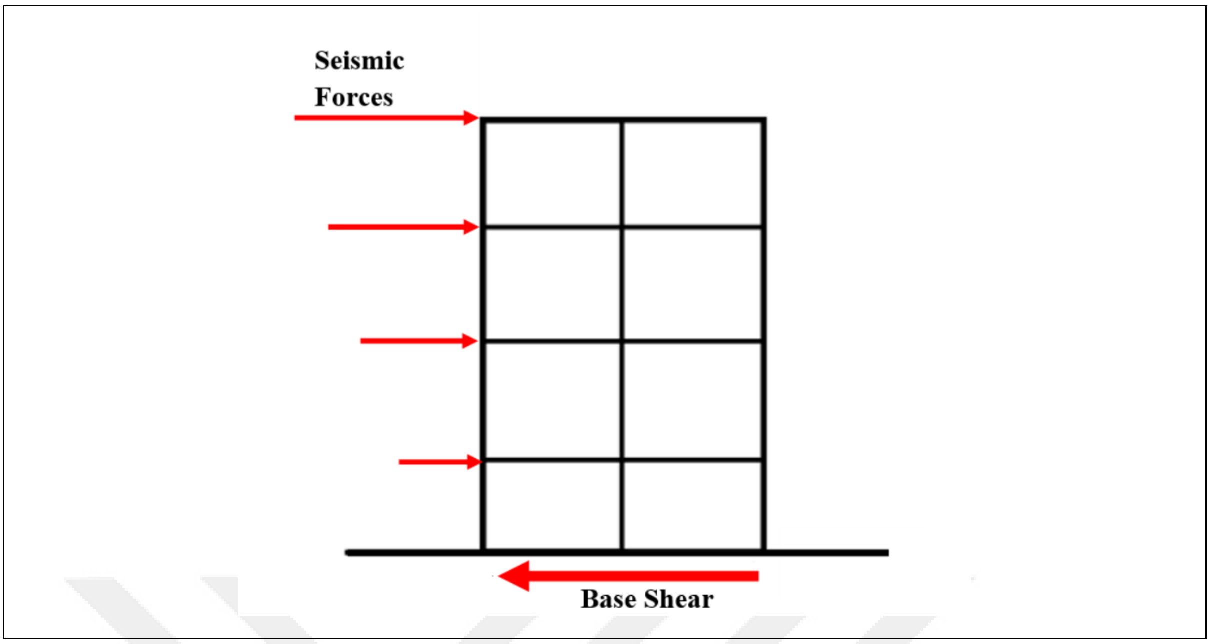

Figure 3.3: Base Shear.

3.1.8 Factor of Importance

It is required that each structure be given an Importance Factor, denoted by Ie, and discussed in Table 3.2.

Table 3.2: The Flooding, Storm, Tornado, Snowfall, Quake, and Ice Load Categories are Assigned to Structures and Buildings According to Their Risk.

Use purpose	**Category of Risk**
In the event of their collapse, buildings which pose a minimal threat to human life are considered safe.	I
Every building, with the exception of those that are designated in Risk Types I, III, and IV	II
Types of buildings, the collapse of which could represent a significant threat to human life	III
The term "essential facilities" can be applied to a variety of different types of buildings.	IV

Table 3.3: *Ie* Factor Based on Table 3.2.

Category of Risk	***Ie***
I	1
II	1
III	1.25
IV	1.5

3.1.9 Torsional Irregularity

When the maximum story drift, calculated taking unintentional torsion into account, occurs during one end of the building transverse to an axis and is larger than 1.2 times that average of the story drifts at the opposite edges of the structure, torsional irregularity is present. This is the definition of torsional irregularity. Only buildings with rigid or semi-rigid diaphragms are subject to the criteria for torsional irregularity in their structures.

3.1.10 Extreme Torsional Irregularity

Extreme torsional irregularity is defined as existing when the highest story drift, calculated which include accidental torsion, at one end of the building transverse to such an axis is larger than 1.4 times the mean of the story drifts somewhere at two ends of the structure. This definition applies only when the maximum story drift is measured at one end of the structure. Only structures with rigid or semirigid diaphragms are capable of having extreme torsional irregularities.

3.2 THE RESPONSE COEFFICIENT CALCULATION

Method 1 or Method 2 may be used to calculate the seismic response coefficient, Cs, in situations in which the original spectral acceleration variable Sa was computed in line with either Chapter 11.4.5.1 (ASCE 7-22). Method 1 and Method 2 must both adhere to the lower bound specified for the linear dynamic response parameter, Cs, which is specified in Item 3.

3.2.1 Method 1

The dynamic loading coefficient, denoted by Cs, is to be calculated using the equation that is provided in the next equation.

$$C_s = \frac{S_a}{\left(\frac{R}{I_e}\right)} \tag{3.2}$$

Here,

Sa is the response acceleration variable that is defined in the Chapter 12.8.2 (ASCE 7-22);

R represents the response modification factor in Table 3.4 (ASCE 7-22); and

Ie is the Importance Factor which can be determined through Table 3.2.

Table 3.4: Table Response Modification Factor co-Efficient.

Structural System	**R**
RC shear walls (special)	5
RC ductile coupled walls	8
Ordinary RC shear walls	4
Braced frames	8
Special RC shear walls	6
RC ductile coupled walls	8
RC shear walls (ordinary)	5
RC moment frames (special)	5
RC moment frames (intermediate)	3
Ordinary RC moment frames	8

3.2.2 Method 2

The coefficient, Cs, have to be calculated following the equation below.

$$C_s = \frac{S_{DS}}{\left(\frac{R}{I_e}\right)} \tag{3.3}$$

Here,

S_{DS} = Design spectral response acceleration parameter

3.3 THE FUNDAMENTAL TIME PERIOD

The fundamental time limit of the building, T, in the plane that is being considered must be determined by performing an analysis that is sufficiently supported and making use of the structural qualities and deformational features of the components that are resisting deformation. The fundamental period, T, must not be longer than the combination of the variable for the maximum bound on computed period, Cu, which can be found in Table 3.5, and the estimated fundamental period, Ta, which can be calculated by using the equation that is provided in the next sentence.

$$T_a = C_t h_n^x \tag{3.4}$$

Table 3.5*:* Determination of Parameter Cu.

Spectral Acceleration at 1 s	**Coefficient Cu**
≥ 0.4	1.4
0.3	1.4
0.2	1.5
0.15	1.6
≤ 0.1	1.7

3.4 RESPONSE SPECTRUM ANALYSIS (RSA)

The estimation of the structural response to brief, nondeterministic, time - dependent events can be accomplished through the use of a technique known as response spectrum analysis. Earthquakes and shocks are two examples of these types of phenomena. Because the precise time history of the load cannot be determined, it is difficult to carry out an analysis that is time-dependent. The brief duration of the event precludes the possibility of treating it as an ergodic (or "stationary") process; hence, a random response strategy is not appropriate for this situation. either.

The response spectrum approach utilizes a specialized kind of mode superposition as its fundamental building block. The purpose of providing this input is to establish a limit for the amount that an eigenmode with a specific resonance frequencies and damping may be aroused by an action of this kind.

Types of RSA

a. (SDOF)- Single Degree of Freedom System

b. (MDOF)- Multiple Degree of Freedom System

3.4.1 Analysis of an SDOF System

Take into consideration a mass-spring-damper system that is attached to a base that is moving. The base possesses a predetermined movement denoted by b(t) (Figure 3.7).

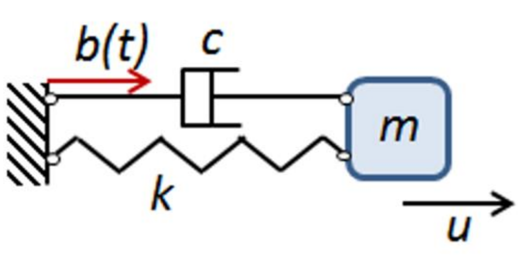

Figure 3.4: SODF System.

If there are no forces acting on the mass from the outside, the motion equation for the mass may be stated as

$$m\ddot{u} + c(\dot{u} - \dot{b}) + k(u - b) = 0 \tag{3.5}$$

Using the conventional system of notation and splitting by the weight,

$$\ddot{u} + 2\zeta\omega_0\dot{u} + \omega_0^2 u = 2\zeta\omega_0\dot{b} + \omega_0^2 b \tag{3.6}$$

In this case, the natural (angular) frequency that is undamped is

$$\omega_0 = \frac{c}{2\sqrt{km}} \tag{3.7}$$

Where the damping ratio,

$$\zeta = \frac{c}{2\sqrt{km}} \tag{3.8}$$

It is clear that the endorse movement performs the function of a forcing term, while the result requires solely on the two variables ζ and, and not on the specific factors m, c, and k. This may be observed for yourself by looking at the diagram.

It is possible to pick the comparative deformation seen among the mass and the base as the degree of freedom, which is denoted by the equation, $u_r = u - b$.. This is an alternative to choosing the relative displacement as the freedom degree. In reality, this is a frame transformation in which the oscillator is investigated using a coordinate system that is attached to the base. There will always be inertial forces present in any frame that is speeding. It is possible to express the motion equation as

$$\ddot{u}_r + 2\zeta\omega_0\dot{u}_r + \omega_0^2 u_r = -\ddot{b} \tag{3.9}$$

As a result, the acceleration of the support seems to be a weight similar to gravity. This depiction offers two distinct benefits, which are as follows:

a. The internal forces of the system, which include elastic and damping forces, are dependent on the respective displacements and velocities of the system's components. A motion of a rigid body has no effect on these forces.

b. In many cases, the data that has been measured is presented in the form of an accelerogram; hence, the underlying deformations are still not available directly.

This equation may be computed for a reasonably long period of time for a variety of different combinations of ω_0, ζ and *b(t)*. The optimum value that are induced by the acceleration history b are utilized to define the movement, motion, and elastic response spectra b(t).

$$S_d(\omega_0, \zeta, b(t)) = max_t |u_r(t)| \tag{3.10}$$

$$S_v(\omega_0, \zeta, b(t)) = max_t |\dot{u}_r(t)| \tag{3.11}$$

$$S_a(\omega_0, \zeta, b(t)) = max_t |\ddot{u}_r(t)| \tag{3.12}$$

Through the utilization of the relative movement u.

$$S_{d+}(\omega_0, \zeta, b(t)) = max_t u_r(t) \tag{3.13}$$

$$S_{d-}(\omega_0, \zeta, b(t)) = min_t u_r(t) \tag{3.14}$$

It is common practice to approximation the motion and acceleration response spectra using

$$S_v \approx \omega_0 S_d \tag{3.15}$$

$$S_a \approx \omega_0^2 S_d \tag{3.16}$$

As this types typically called pseudo velocity and pseudo acceleration spectra.

The pseudo acceleration spectrum that is calculated using the relative movement is in fact equivalent to the actual acceleration spectrum when applied to a system that does not include any damping. This may be demonstrated by looking at the equation below

$$\ddot{u}_r + \omega_0^2 u_r = -\ddot{b} \tag{3.17}$$

So,

$$\omega_0^2 u_r = -\left(\ddot{b} + \ddot{u}_r\right) = -\ddot{u} \tag{3.18}$$

Therefore, the point in time at which the highest magnitude of the relative motion coincides with the point in time at which the highest upper bound of the relative acceleration must take place. The scale factor that differentiates the two is denoted by ω_0^2. This correlation will remain roughly valid even for systems that have a low level of dampening. It is typical to make the assumption that such spectra for the actual acceleration as well as the pseudo acceleration are identical. This is due to the fact that the majority of propulsion parts have a low damping (generally 2% to 5%).

The Q factor is an additional frequent method that is used to describe the absorption in this situation. The equation that describes the connection to that same damping ratio is as follows:

$$Q = \frac{1}{2\zeta} \tag{3.19}$$

3.4.2 Multiple DOF System

Let's say a numerical equation of a structure is segmented using FEM in such a way which the motion equations in matrix form are as follows:

$$\mathrm{M\ddot{u}} + \mathrm{C\dot{u}} + \mathrm{Ku} = \mathrm{f}(t) \tag{3.20}$$

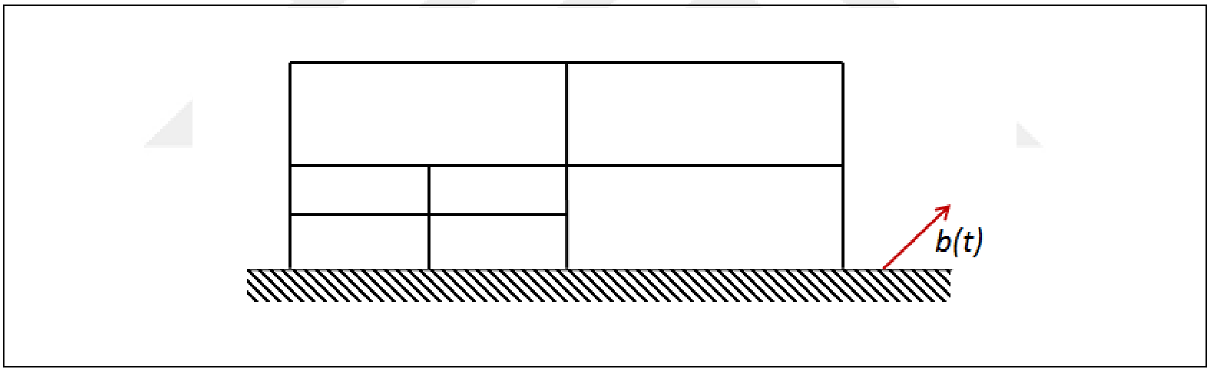

Figure 3.5: MDOF System.

The base motion of the building is determined by the fact that it is connected at a variety of locations to a single "ground" (t). This vector is the same size as **u** , which represents the entire number of DOFs; however, it only includes three distinct characteristics: : $b_x(t)$, $b_y(t)$, and $b_z(t)$. Now, the entity is denoted by the notation $\mathbf{u}_r = \mathbf{u} - \mathbf{b}$. If there is no load from the outside, the motion equation is.

$$\mathrm{M}(\ddot{\mathrm{u}}_r + \ddot{\mathrm{b}}) + \mathrm{C}\dot{\mathrm{u}}_r + \mathrm{K}\mathrm{u}_r = 0 \tag{3.21}$$

or

$$\mathrm{M}\ddot{\mathrm{u}}_r + \mathrm{C}\dot{\mathrm{u}}_r + \mathrm{K}\mathrm{u}_r = -\,\mathrm{M}\ddot{\mathrm{b}} \tag{3.22}$$

Here, viscous forces in the system is used, as a result, $\mathrm{Kb} = \mathrm{C}\dot{b} = 0$

By solving $(\mathrm{K} - \omega^2\mathrm{M})\phi = 0$

$$\Phi = [\phi_1 \phi_2 \quad \dots \quad \phi_N] \tag{3.23}$$

In accordance with the conventional procedures for modal overlap, the decoupled modal solutions are as follows:

$$\ddot{q}_j + 2\zeta_j\omega_j\dot{q}_j + \omega_j^2 q_j = -\phi_j^T\mathrm{M}\ddot{\mathrm{b}} \tag{3.24}$$

It has been taken for granted that perhaps the weight matrix normalizing of the eigenmodes will be applied, as well as the damping matrix will be able to be diagonalized mostly by eigenmodes. The normalizing of the mass matrix is not required, however doing so will make some formulas easier to understand.

Here, qj denotes the fundamental coefficient for mode j; hence, one may express the relative displacement as a linear function of eigenmodes, with the weighting determined mostly by modal coordinate values:

$$\mathrm{u}_r = \Phi\mathrm{q} \tag{3.25}$$

The support motion

$$\mathrm{b}(t) = b_x(t)1_x + b_y(t)1_y + b_z(t)1_z \tag{3.26}$$

The number "1" is assigned to all degrees of freedom (DOFs) that pertain to X-translation, whereas the value "0" is assigned to all other DOFs. Therefore, the equation of motion for modes of motion is.

$$\ddot{q}_j + 2\zeta_j\omega_j\dot{q}_j + \omega_j^2 q_j = -\phi_j^T\mathrm{M}\big(\ddot{b}_x(t)1_x + \ddot{b}_y(t)1_y + \ddot{b}_z(t)1_z\big) = -\Gamma_{xj}\ddot{b}_x(t) - \Gamma_{yj}\ddot{b}_y(t) - \Gamma_{zj}\ddot{b}_z(t) \tag{3.27}$$

Here the multipliers r_{kj}, And,

$$\Gamma_{kj} = \phi_j^T \mathrm{M} 1_k \tag{3.28}$$

Therefore, when loaded by a fundamental motion in the direction k defined by a response spectrum, the peak amplitude of mode j equals

$$\hat{q}_{kj} = S_d\big(\omega_j, \zeta_j, b_k(t)\big)\Gamma_{kj} \tag{3.29}$$

In another words the pseudo acceleration spectrum

$$\hat{q}_{kj} = \frac{S_a\big(\omega_j, \zeta_j, b_k(t)\big)\Gamma_{kj}}{\omega_j^2} \tag{3.30}$$

In a nutshell, the peak amplitude of a particular eigenmode is calculated by multiplying the response spectrum value at the associated natural frequency (which is unaffected by the structure) by the participation factor.

3.5 CALCULATION PROCEDURE OF RSA IN THIS THESIS

3.5.1 Parameters

3.5.1.1 g

It is the gravitational Acceleration

3.5.1.2 Site class

It is required that the soil at the site be categorized in line with Table 3.6.

Site Class F: A soil type that contains soils that are susceptible to probable failure during earthquake loads, such as cohesionless soils, fast and incredibly sensitive clays, and compressible weakly cemented soils, is called a seismically vulnerable soil profile.

Site Class A: Its measured between the hard rock types of soil. These measurements must be performed in order to support the category. These measures may be carried out either on the premises or away from the premises. In regions where it is known that the characteristics of hard rock are continuous down to a depth of one hundred feet or more (30 m)

Site Class B: This sort of terrain will include conditions that are medium hard to soft rock sites.

Site Class E: When a site does not meet the requirements for Site Class F and there is a total thickness of soft clay that is greater than 10 feet (3 meters), and when a soft clay layer is defined as having su that is less than 500 psf (su that is less than 25 kPa), then the site is considered to be in Site Class G.

Table 3.6: Site Class Values.

Site Class	**Vs**
Hard rock	greater than 5,000
Medium hard rock	In between 3,000 to 5,000
Soft rock	In between 2,100 to 3,000
Medium dense sand or stiff clay	In between 700 to 1,000
Loose sand or medium stiff clay	In between 500 to 700
Very loose sand or soft clay	Less than 500

3.5.1.3 R

According to Table 3.4 of Design Coefficients and Factors for Seismic Force-Resisting Systems, the response modification coefficient.

3.5.1.4 Risk category

The risk coefficient was calculated based on Table 3.1.

3.5.1.5 Importance factor (Ie)

Importance factor is calculated according to Table 3.2

3.5.1.6 Seismic design category

Earthquake Design Class E must be allocated to any building in a region with a Risk Category I, II, or III if the calculated spectral response acceleration constant at the 1-s interval, S1, is more than or equal to 0.75. Structures belonging to Risk Category IV that are located in areas in which the estimated spectral response acceleration factor at 1-s period, S1, is more than or equal to 0.75 must be classified as belonging to Seismic Design Category F. The seismic design category that should be applied to every other structure is determined by the risk level associated with it as well as the designed spectral response acceleration parameters, Ss and S_1, that are calculated. The seismic design category according to Table 3.7 is given below.

Table 3.7: Table for Determining Ss.

Site Class	$S_s \leq 0.25$	$S_s = 0.5$	$S_s = 0.75$	$S_s = 1.0$	$S_s \geq 1.25$
A	0.8	0.8	0.8	0.8	0.8
B	1	1	1	1	1
C	1.2	1.2	1.1	1	1
D	1.6	1.4	1.2	1.1	1
E	2.5	1.7	1.2	0.9	0.9

3.5.1.7 Evaluation of response spectrum

The following requirements should be attained by the design RSA

a. At period, T, equal to 0 seconds, 0.01 seconds, 0.02 seconds, 0.03 seconds, 0.05 seconds, 0.075 seconds, 0.1 seconds, 0.15 seconds, 0.2 seconds, 0.25 seconds, 0.3 seconds, 0.4 seconds, 0.5 seconds, 0.75 seconds, 1.0 seconds, 1.5 seconds, 2.0 seconds, 3.0 seconds, 4.0 seconds, 5.0 seconds, 7.5 seconds, and 10 seconds, the 5%-damped design RS parameter, Sa.

b. If the reaction time, T, is shorter than 10 seconds but is not equal to any of the discrete data of period, T, provided in Item 1 above, then Sa is selected by linear interpolation between both the values of Sa, of Item 1 above.

c. If T ≤ T_L, Sa is calculated as even the rate of Sa just at period of 10 s of Item 1 above multiplied by 10/T; and where T > T_L, Sa is calculated as that of the value of Sa at the period of 10 s multiplied by 10 T_L/T_2.

d. The value of the model spectral response acceleration variable, Sa, is to be determined in accordance with the equation that is shown in the next paragraph.

$$S_a = S_{DS}\left(0.4 + 0.6\frac{T}{T_0}\right) \tag{3.31}$$

i. The model spectral response acceleration factor, S_a, is to be taken as equal to S_{DS} for all periods that begin after T_0 and end before T_s. This applies to all periods that begin after T_0 and end before T_s.

ii. The model spectral response acceleration factor, S_a, should be regarded as indicated in the following equation for periods that are higher than T_s and smaller than or equivalent to T_L.

$$S_a = \frac{S_{D1}}{T} \tag{3.32}$$

iii. The Periods higher than T_L, S_a shall be taken as given in the following equation.

$$S_a = \frac{S_{D1}T_L}{T^2} \tag{3.33}$$

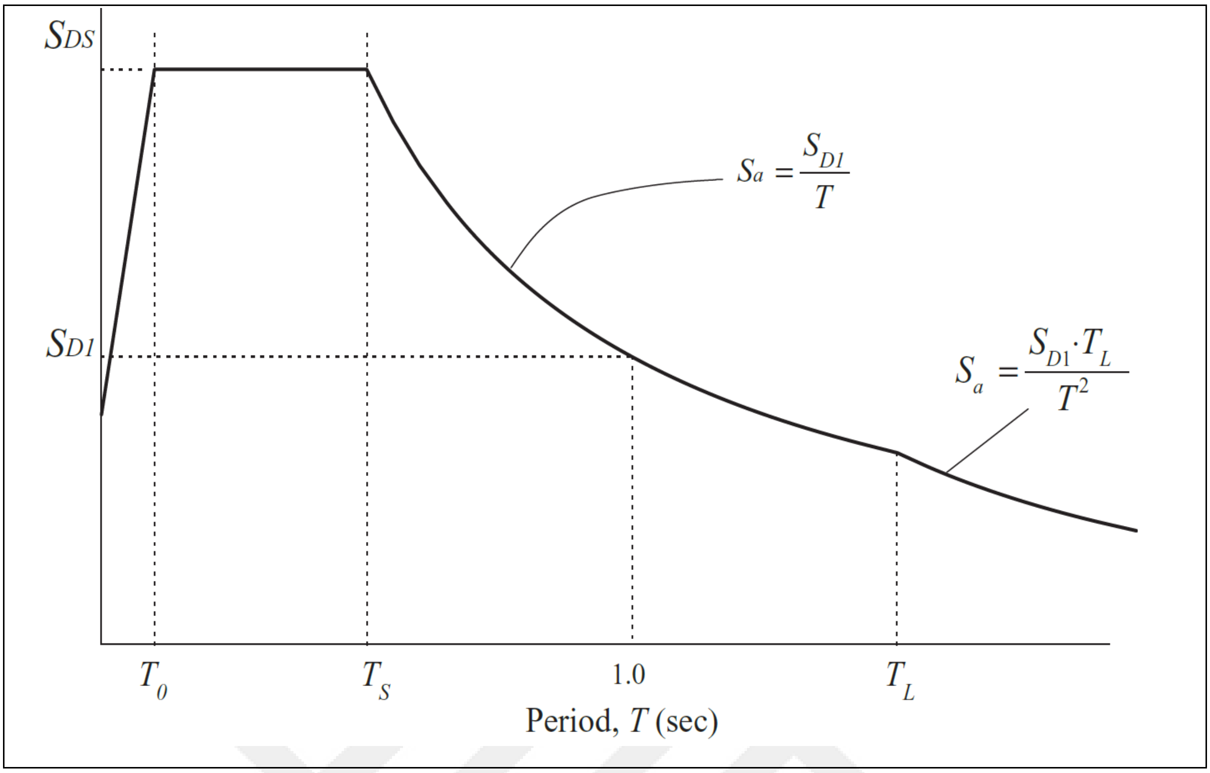

Figure 3.6: Parameters for Design Spectrum.

3.5.1.8 Maximum value of T

$$T_{max} = C_u T_a \tag{3.34}$$

Cu is taken from Table 3.5

The following is an approximation of the basic time periods that buildings have existed:

$$T_a = C_t h_n^x \tag{3.35}$$

Here,

T_a is the estimate time period

h_n represents the height of the top to the reference floor.

C_t as well as the value x obtained from Table 3.8

Table 3.8: Coefficient for Ct and x.

Structure	***C_t***	***x***
Steel MRF system	0.0724	0.8
Concrete MRF system	0.0466	0.9
Every single one of the other structural systems	0.0488	0.75

3.6 TIME HISTORY ANALYSIS

Equivalent static force method is one of the easiest solutions for carrying out linear dynamic analysis and serves as a representation of linear static analysis. That straightforward approach adheres to formulas provided in the practice guidelines as well as involves minimal computing work. Conversely, it also applies to specified structural system categories having standardized geometries and capped heights [84]. Response spectrum analysis is also far more efficient than a static equivalent when utilized as a linear dynamic method [85]. The preferred method to assess structural behavior under seismic events defined through ground velocity data is time-history analysis, a nonlinear dynamic analysis. One of most potent method for nonlinear analysis, process integrations, is used to resolve the fundamental motion equations for active seismic forces that sequentially influence the building throughout different intervals Δt. A number of brief time intervals are used to assess the reaction. The fundamental motion formula is:

$$\mathrm{M\ddot{U}(t) + C\dot{U}(t) + KU(t) = -M\ddot{U}_g(t)} \tag{3.36}$$

Here,

M denotes the mass, C denotes the damping and K denotes the stiffness matrices,

The initials U, $\dot{U}$ and $\ddot{U}$, respectively, stand for the vectors of movement, speed, and acceleration. The ground's acceleration vector is $\ddot{U}_g$. Through setting the appropriate interpolated formula, these above vectors as well as matrices can be computed for a single-dimensional component [86]. The progressive format of the equation is as follows:

$$M\Delta\ddot{U}(t) + C(t)\Delta\dot{U}(t) + K(t)\Delta U(t) = \Delta P(t) \tag{3.37}$$

Here,

The incremental displacement, velocity, and acceleration vectors are designated by the symbols $\Delta U(t)$, $\Delta\dot{U}(t)$ and $\Delta\ddot{U}(t)$, correspondingly. The outer seismic pressure's incremental vector is represented by the vector $\Delta P(t)$.

The approach presented by Chen and Robinson [87] eliminated any restriction upon this size of time frames as well as enables lengthier periods, even if the time intervals must be small enough to offer a precise image of a rapidly moving time-dependent function when using standard means. The implicit and explicit Runge-Kutta approaches are the foundation of other strategies for resolving basic motion equations progressively [88, 89]. The dynamical evaluation of the present investigation will be carried out using a ground stimulation. These data were collected in El Centro, nearby the fault, in 1940, at a geographical originating distance of around 8 kilometers. The velocity time records for the two ground motion earthquakes considered in this investigation are shown in Figure 3.7. The PEER Strong Motion Database is where the ground shaking data are found.

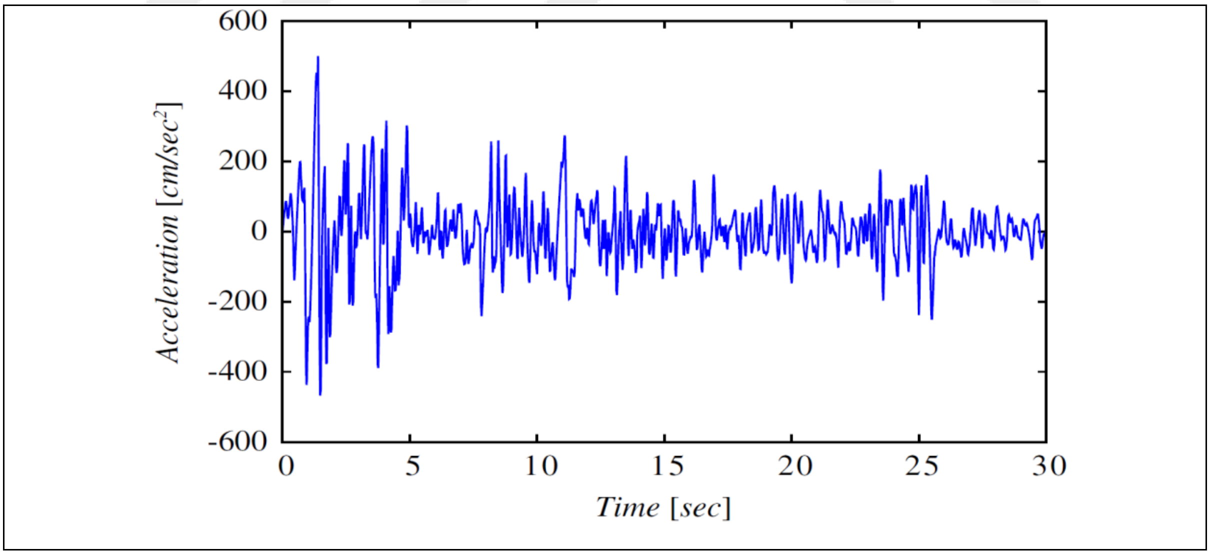

Figure 3.7: El-Centro Seismic Wave Acceleration Time History.

3.6.1 Characteristics of The Seismic Signal

The earthquake pressures inside a building are often generated by the speed of ground movement. Using two building models, a dynamic time history evaluation was carried out. Understanding overall dynamic behavior of the structure under actual seismic load is made possible through this kind of research. Figure 3.7 shows the results of the nonlinear time history assessment both in the X and Y directions using the El Centro (1940) data [90].

The 1940 El-Centro ground motion had been observed at a ground area about 8 km from the fault's surface propagation throughout an M-6.9 strike-slip seismic. The El Centro data is available in a number of variations [91, 92]. Among the earlier and most popular relatively close ground movement is the El-Centro ground motion. The records of acceleration, speed, and movement don't really include any pulses. The maximal ground acceleration for the two model structure is 0.508 g, and the ground motion has a time evolution of 30 seconds. At a time, interval of 0.02 seconds, full earth accelerating VS time record was accessible. El Centro ground motion's amplitudes regarding ground acceleration, velocity, and displacement (PGA, PGV, and PGD) are as follows: PGA = 0.32 g, PGV = 36 cm/s, and PGD = 21 cm [93]. The work of Mollaioli et al and Mustafa and Takewaki [94, 95] could serve as a foundation for additional ground shaking variables for El Centro, such as accumulative velocity IV, earthquake risk power factor AE1, as well as maximum power spectral ordinate (E1) max, pertinent towards the fault-normal FN, and fault-parallel FP, aspects of a ground movement.

3.7 STRUCTURAL MODEL

ETABS is utilized in order to carry out the analysis for the plan of the high-rise construction. In the course of the research, a rectangular floor design for a high-rise building of twenty stories was taken into consideration. The third-dimensional finite element analysis was applied to a total of three different models, including RCC Moment Resisting Frame (MRF) model [Figure 3.8], Core shear wall model [Figure 3.9], Bracing frame model [Figure 3.10]. The models are denoted as Case-1, Case-2 and Case-3 respectively.

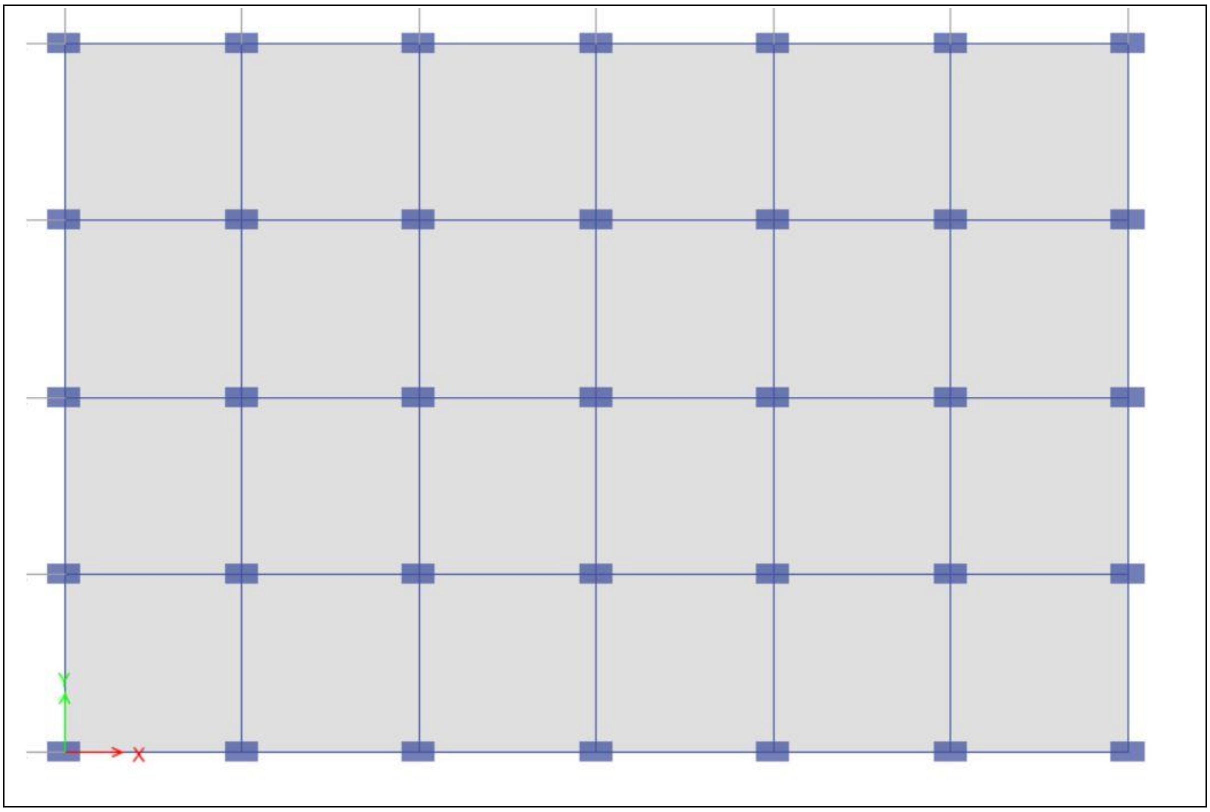

Figure 3.8: Moment Resisting Frame Model (Case-1).

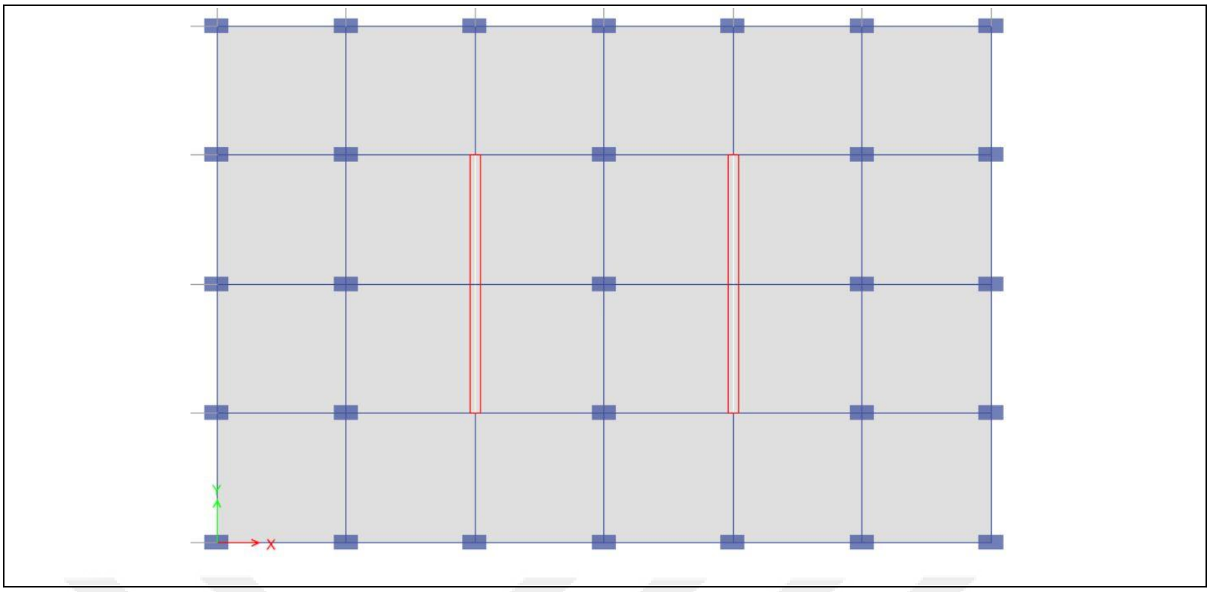

Figure 3.9: Core Shear Wall Model (Case-2).

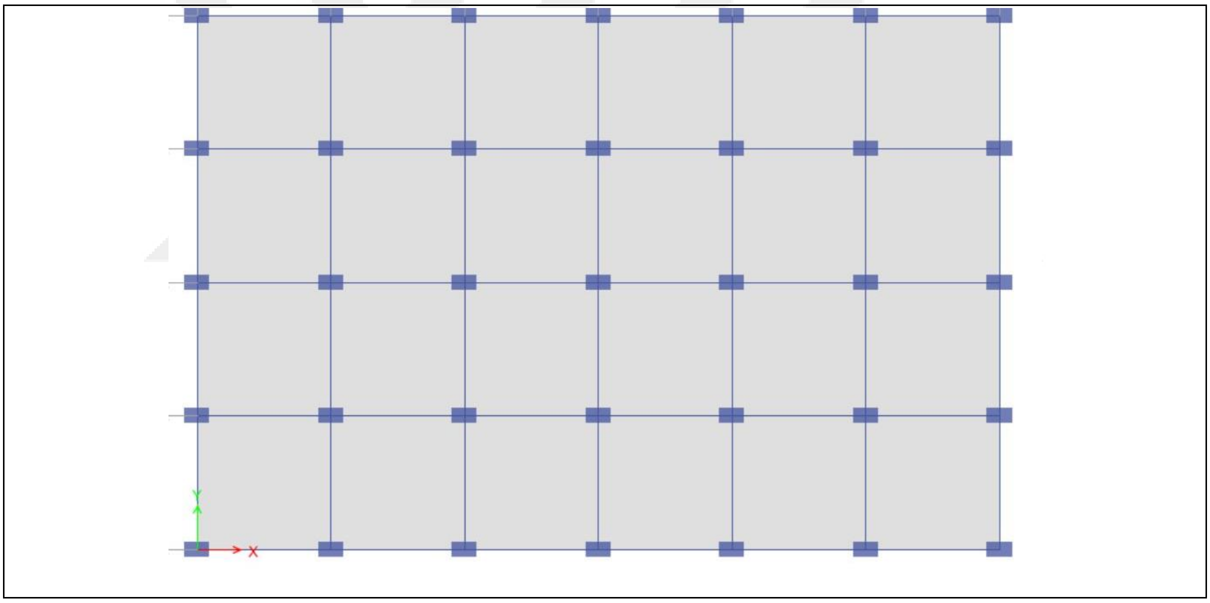

Figure 3.10: Steel Bracing Model (Case-3).

Figure 3.11, Figure 3.12, and Figure 3.13 each show an illustration of the three-dimensional elevations of the Case-1, Case-2, and Case-3 models, respectively.

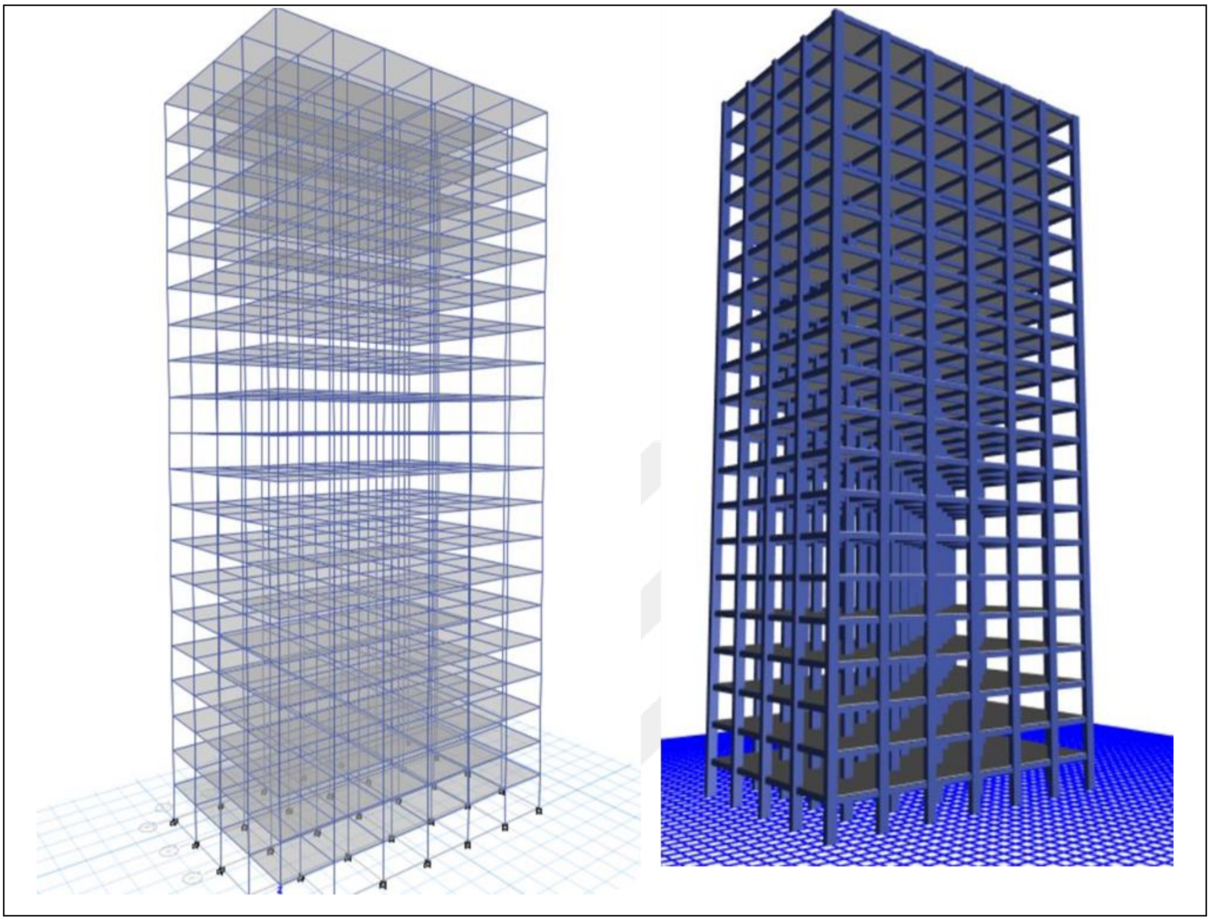

Figure 3.11: 3-D view of Case-1.

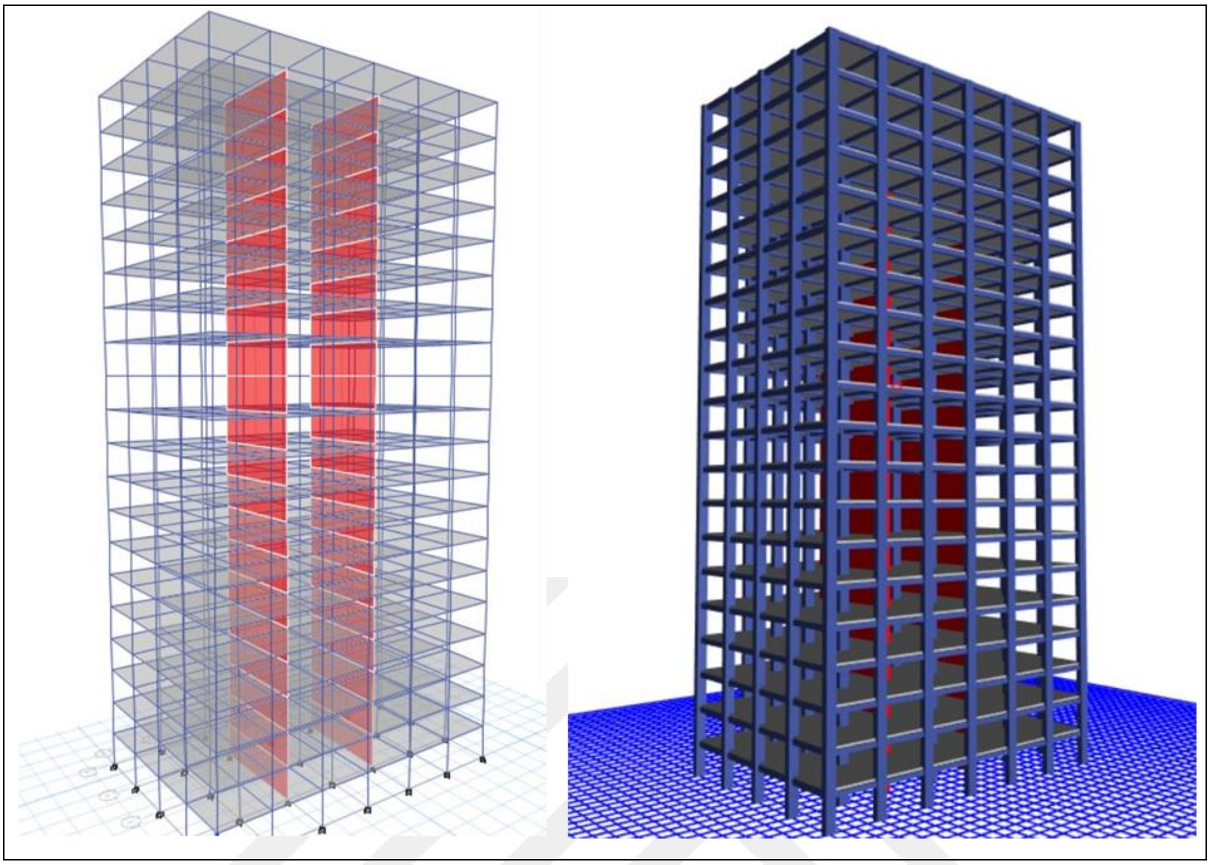

Figure 3.12: 3-D View of Case-2.

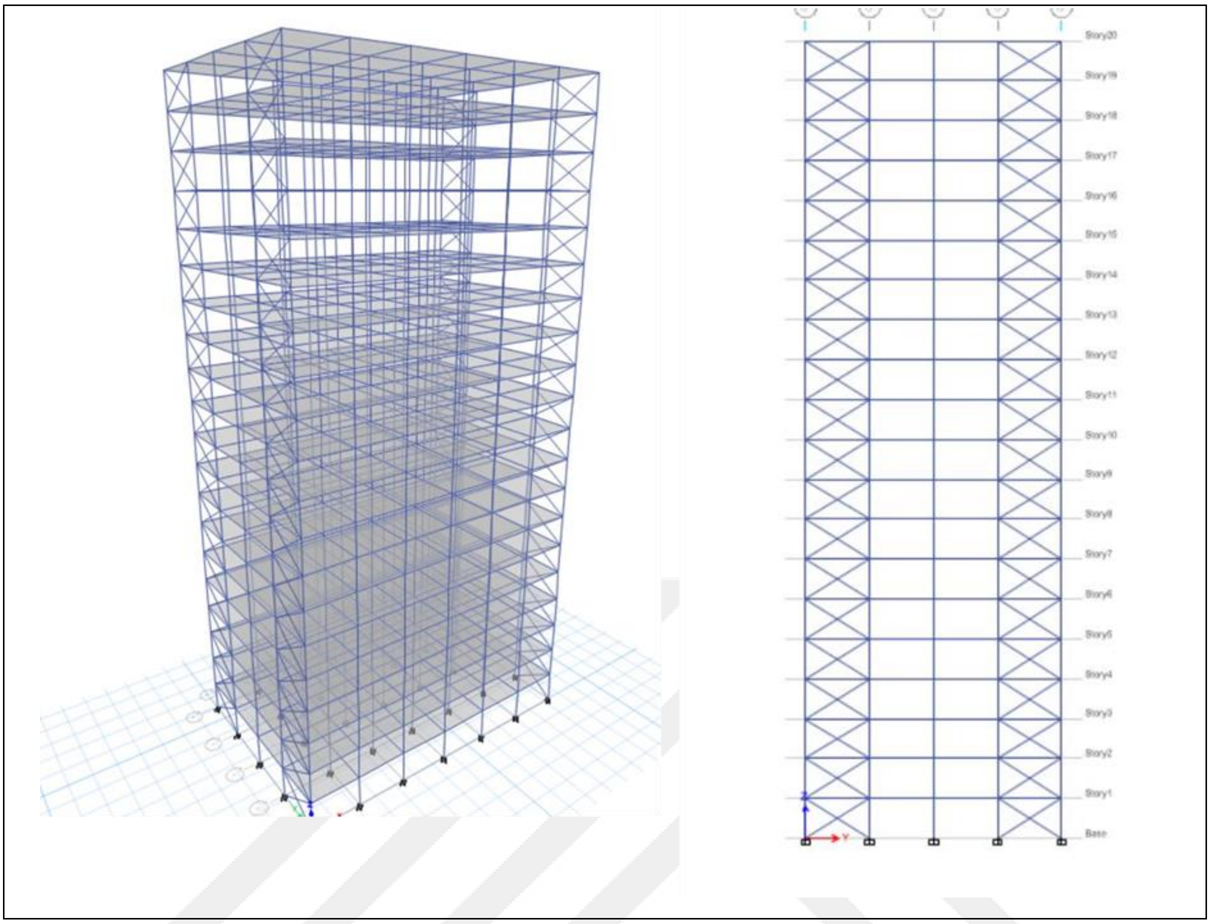

Figure 3.13: 3-D view and Bracing Orientation of Case-3.

3.7.1 Material Properties

In this particular analysis, the grade of concrete known as C35 was employed for the columns and shear walls of all of the mathematical models, while the grade known as C30 was utilized for the beams, slabs, and outrigger systems. Table 2 outlines the material properties of both the concrete and the steel reinforcement used in the construction. In every model, the slab thickness was determined to be 175 millimeters, and the column dimension was determined to be 600 millimeters by 900 millimeters. In addition, a beam depth of 450 millimeters was taken into consideration.

Table 3.9: Mechanical Properties of The Materials.

Material	E (MPa)	ν	Density (kg/m^3)	ε_u	Compressive strength (MPa)	F_y (MPa)	F_u (MPa)
C35	27777	0.18	2400	0.002	35	-	-
C30	25709	0.18	2400	0.002	30	-	-
Rebar	210000	0.2	7850	0.3		250	420

3.7.2 Loading Data

In this investigation, the models are analyzed considering the linear dynamic analysis in accordance with the requirements of ASCE 7-22. (ASCE-7-22, 2022). In this investigation, the service dead load was determined to be 3.5 kN per square meter for each model, and the live load was determined to be 4.0 kN per square meter.

3.7.3 Analysis Procedure

Calculating the maximum response value in each mode of a structure using a spectrum curve is the first step in the Response Spectrum method. Once this value has been determined, the method integrates the responses using model superposition. In general, a building's response is the combination of multiple modes, and the Square Root Sum of the Square technique was utilized in this particular instance. According to ASCE, [96] code spectral acceleration data was developed once the modal load case was specified (Figure 3.14). Following that, the data were reformatted into ETABS using the textual format. The data for all of the seismic zones were generated using the soft soil condition Sc as the basis. A response spectrum load case was defined after performing a linear static analysis. The initial scale factor was taken I_g/R, where ‘g’ is the acceleration due to gravity, ‘I’ is the importance factor and ‘R’ is the response modification coefficient for different frame categories specified in the above sections. A modal analysis was performed for all the models based on the data. In light of the fact that the code permits a minimum of 90% of the static base shear, the scale factor was modified once more after the analysis was carried out. Because the rule requires a minimum modal mass participation ratio of 90%, the mode number was also altered in order to comply with this requirement. Following each and every revision, the mathematical models underwent a fresh analysis in accordance with the ASCE code.

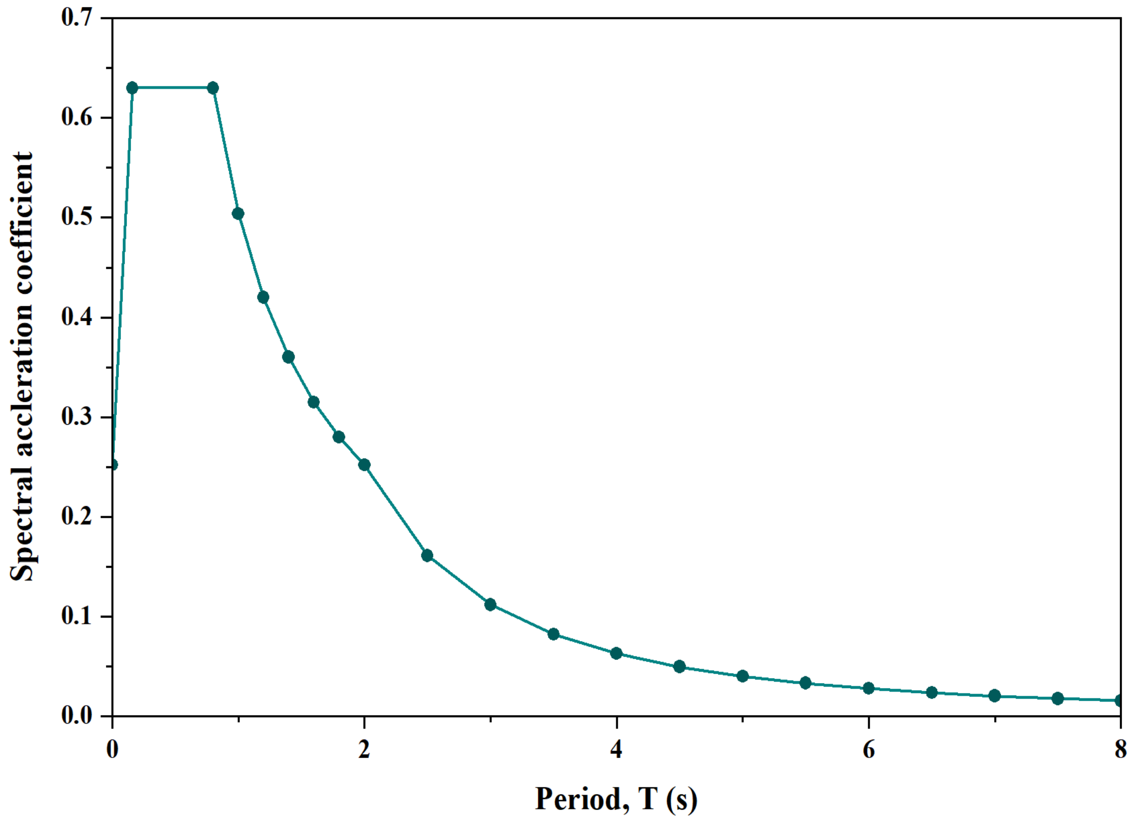

Figure 3.14: Period vs Spectral Acceleration Curve.

Following the completion of the dynamic analysis, both Case-2 and Case-3 data sets underwent the non-linear dynamic analysis, also known as the time history assessment (THA). The Takeda hysteretic model was used for the nonlinear TH studies that were done in this article. When it comes to accurately expressing the nonlinear relationship that exists between both the force applied as well as the associated deformation of both the structural components, this model is often regarded as being among the very finest of those that adhere to hysteretic laws. Figure 3.15 provides a diagrammatic illustration of the force–displacement connection equations derived from the Takeda hysteretic model. Because it was one of the most powerful earthquakes in recent history, the acceleration data from the EI-Centro quake were collected so that a reaction could be calculated.

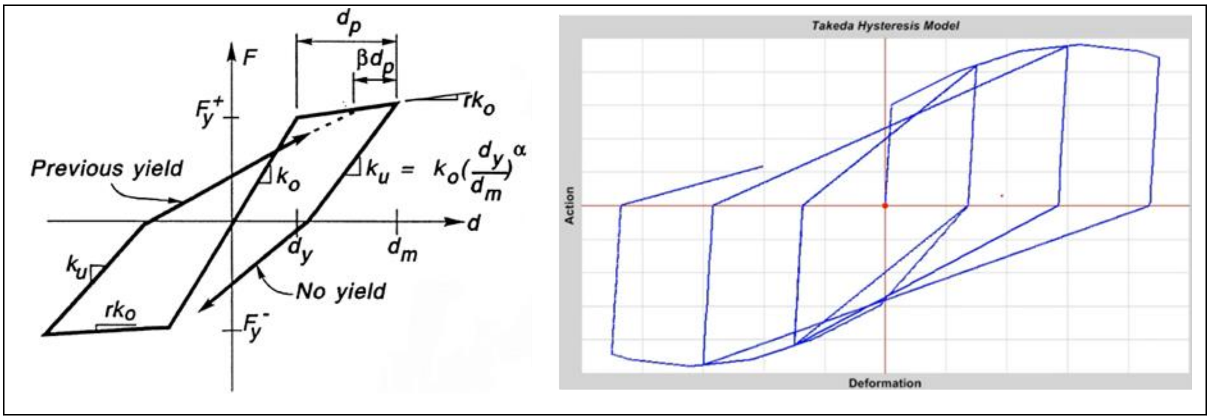

Figure 3.15: The Connection between Force and Deformation, as Well as a Graphic Representation and a Model Constructed in ETABS.

The software model begins with the building's initial stiffness k0 as its starting point. After that, the model is loaded gradually until it reaches its linearity limitations. The construction model enters the nonlinear zone when it surpasses the elasticity limits and arrives just at after yield stiffness rk0. At this point, the iteration process begins to calculate stresses, deflections, and stiffness. dy and dm are the displacements that determine both peak and yielding of the concrete components, respectively.

4. RESULTS AND DISCUSSION

4.1 RESULTS OF LINEAR DYNAMIC ANALYSIS

4.1.1 Story Displacements

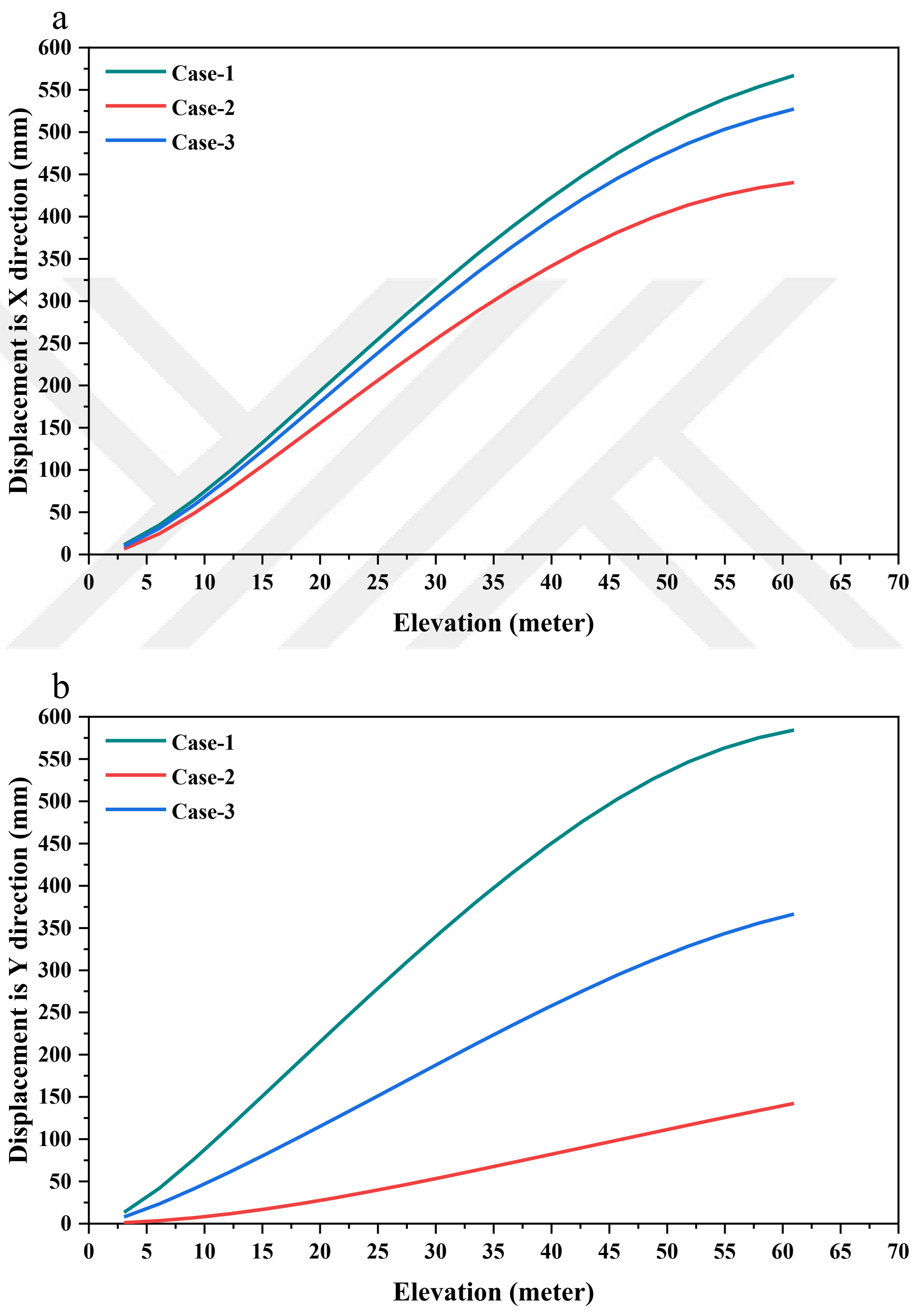

Figure 4.1: Story Displacement at Both Global X and Y Direction.

Figure 4.1 represents the results of story displacement for every model that have been developed. As the dynamic analysis was carried out, the model consisting with shear wall at the core performed better; the displacement was the lowest for this Case-2 in both global-X and global-Y direction. The maximum displacement for this model was 440.42 mm and the lowest displacement was 6.49 mm for global X direction, for global Y direction the maximum displacement was 142.3 mm which is a significant reduction from the global X. On the other hand, Case-3 model consisting of shear bracing systems also depicted great displacement reduction at both directions. The maximum displacement for this model was 527.24 mm and the lowest displacement was 9.50 mm for global-X direction, for global Y direction the maximum displacement was 366.49 mm. However, case-1, consisting of only MRF, showed an average of 28% and 76% higher displacement for both global-X and global-Y direction respectively than the best-performing model at case-2. The maximum displacement for this model was 566.92 mm and the lowest displacement was 11.50 mm for global-X direction, for global-Y direction the maximum displacement was 584.43 mm. Because of the absence of a stiffer system for resisting seismic forces the model consisting only moment resisting frame depicted the highest displacement. The resilient effect of shear wall was also observed by Ahamad and Pratap [97]. The study of Bharti et al. [98] also suggests the effectiveness of bracing system against story displacements. As a result, the combined effect of shear wall both at core and all the corners on case-3 exhibited the best performance against seismic forces.

4.1.2 Maximum Allowable Story Drift

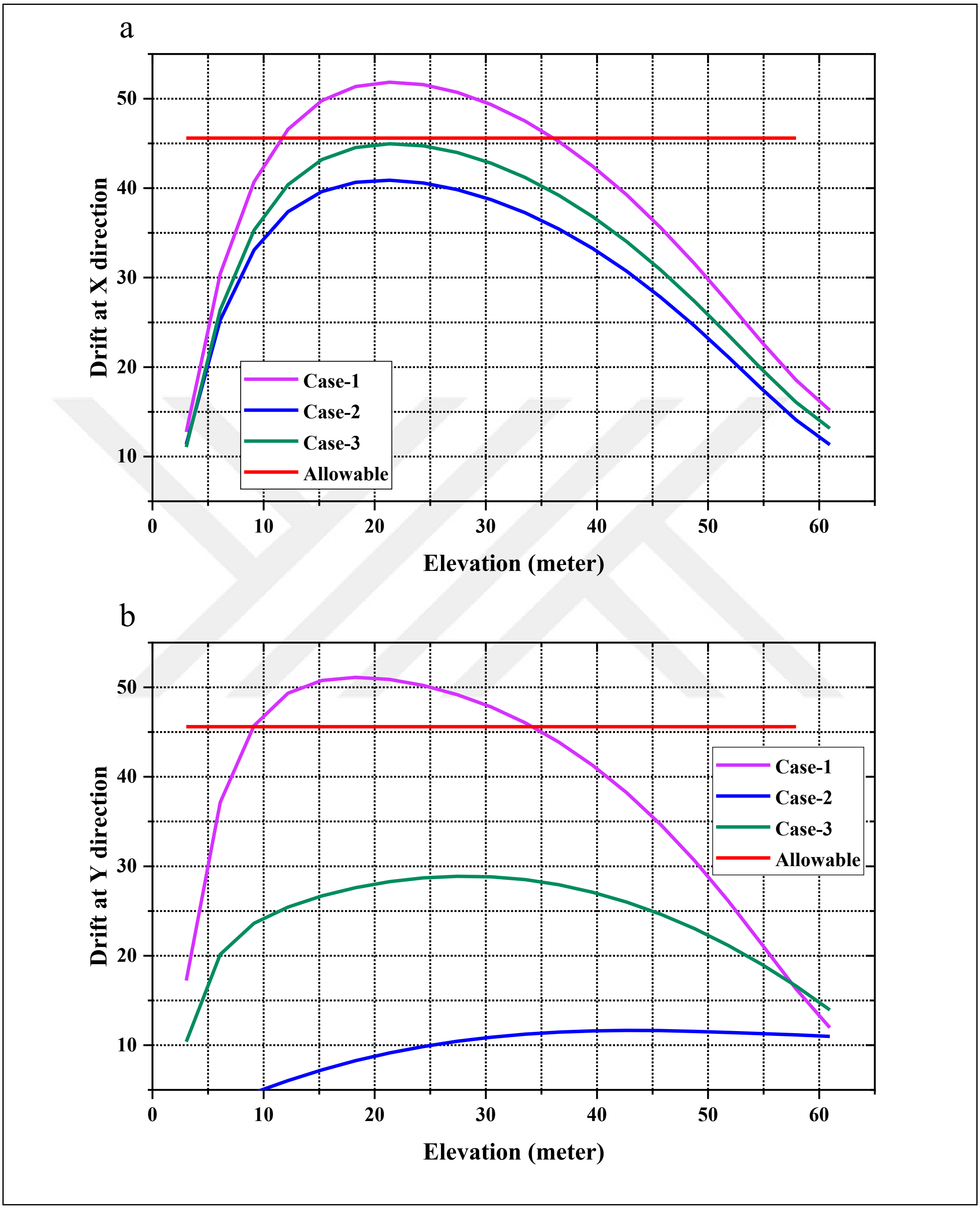

Figure 4.2: Maximum Allowable Story Drift at both Global X and Y Direction.

Figure 4.2 depicts the maximum allowable story drift results for each of the generated models. From the figure it can clearly be seen that the bracing systems and shear wall played an important role to control the drift in both directions. The Case-1 model, which merely had moment resisting frame was not able to control the drift values under the allowable limit. The allowable drift was calculated from the guideline of ASCE 7-22, which is also presented in Table 3.1. The obtained allowable drift value was 45.5. The highest story drift values for Case-1 model were 51.8 and 52.08 whereas the minimum value of the story drift for Case-1 model was 12.75 and 11.95 at the global-X direction and Y direction respectively. The graphical representation illustrates that almost all the story for Case-1 model did not pass according to allowable limit.

On the other hand, the minimum story drift values for Case-3 model was 11.06 and 10.38 while the maximum value was 44.97 and 28.08 at the X and Y direction respectively. Additionally, for Case-2 model, the maximum value of the story drift was 40.88 and 11.64 whereas the minimum value was 11.32 and 1.41 at the X and Y direction respectively. Both Case-2 and Case-3 model consisting shear wall were able to keep the drift under the allowable limit.

4.1.3 Story Drift Ratio

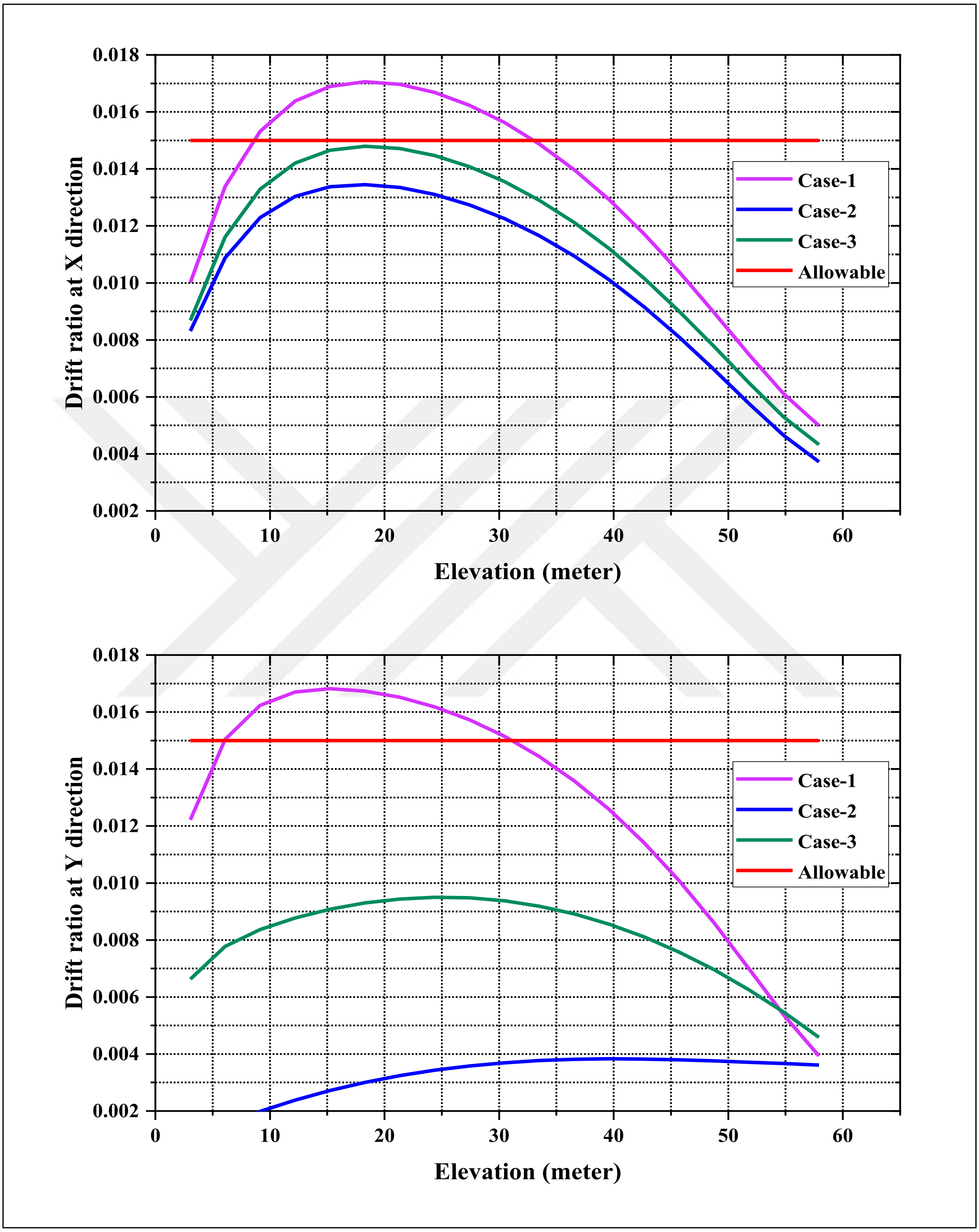

Figure 4.3: Allowable Story Drift Ratio at both Global X and Y Direction.

Figure 4.3 demonstrates the results of the permissible ratio of drifts for every model that have been generated. From the figure it can clearly be seen that both the brace frame and shear wall played an important role to control the drift ratios in the global-X as well as the global-Y directions. The Case-1 model that merely had moment resisting frame was not able to control the drift ratio values under the allowable limit. The allowable drift was calculated from the guideline of ASCE 7-22, which is also presented in Table 3.1. The obtained allowable drift ratio value was 0.015. For Case-1 model, the largest story drift ratio was found 0.017 and 0.0168 while the minimum value was 0.0049 and 0.0039 at both the X and the Y direction, respectively. The graphical representation illustrates that almost all the story for Case-1 models did not pass according to allowable limit.

Besides, the maximum story drift ratio for Case-2 model was 0.013 and 0.0038 at both X and Y direction respectively. On the other hand, the minimum story drift ratio for Case-2 model was 0.0037 and 0.00102 at both X and Y direction respectively. Additionally, for Case-3 model, the maximum value of the story drift ratio was 0.014 and 0.0095 while the minimum value was 0.0043 and 0.0045 at both X and Y direction respectively.

4.1.4 Story Stiffness

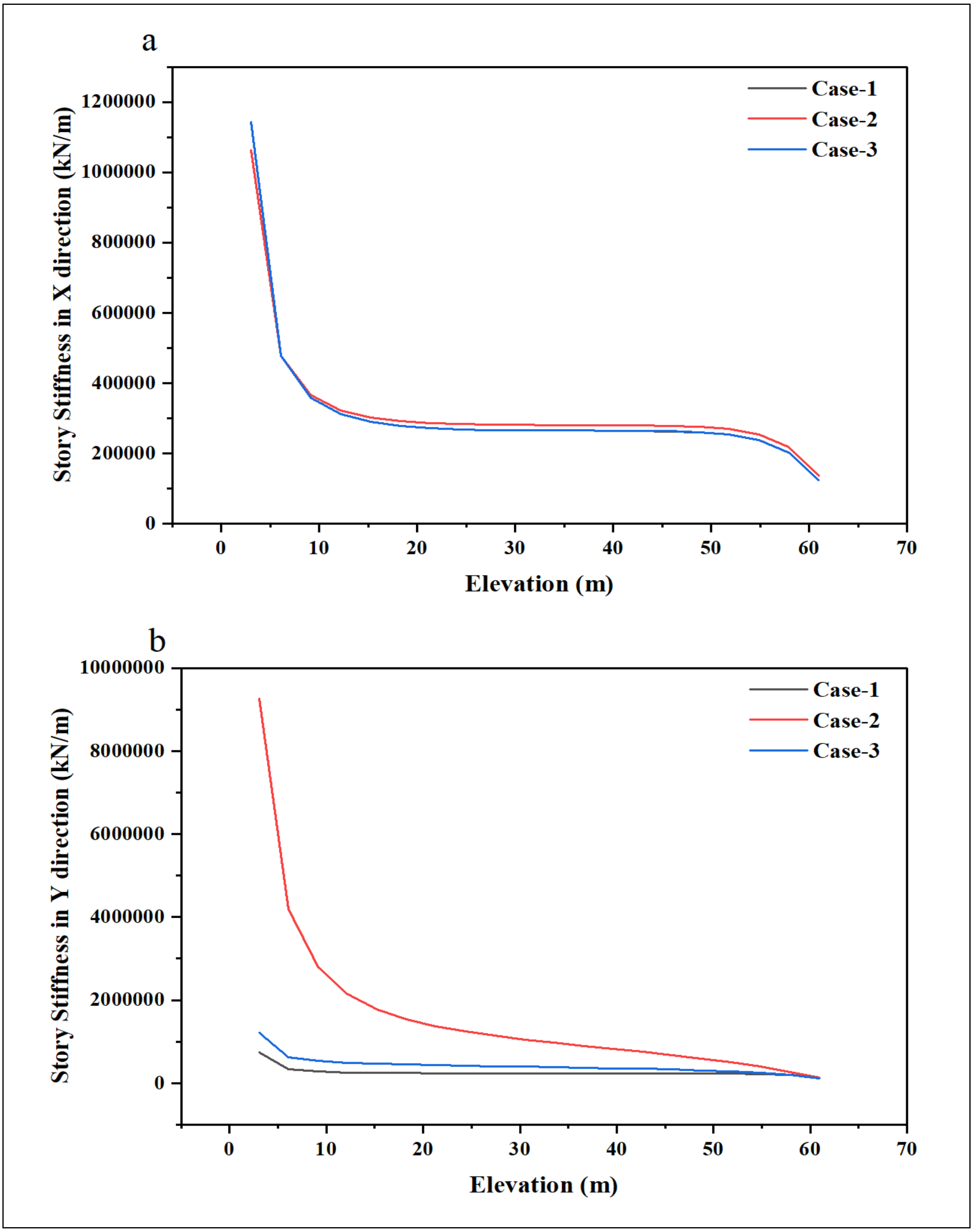

Figure 4.4: Story Stiffness at both Global X and Y Direction.

Figure 4.4 illustrates overall story stiffness values for each of the developed models. The model with the bracing done much better during the dynamic analysis and for the Case-3, the stiffness was highest in both global-X and global-Y direction. The maximum story stiffness for this model was 1142431 kN/m whereas the minimum stiffness was found 123594 kN/m for global X direction, for global Y direction the maximum displacement was 1217306 kN/m which is significantly higher from the global X. The Case-2 model consisting of shear wall at the core also depicted great stiffness enhancement at both directions. The maximum story stiffness for this model was 1064025 kN/m while for global-X direction, the minimum story stiffness was 135056 kN/m and for global Y direction, the maximum stiffness was 9264284 kN/m. However, case-1, consisting of only MRF, depicted the lowest story stiffness. The maximum story stiffness for this model was 1042367 kN/m. On the other hand, the lowest story stiffness was 121503 kN/m for global-X direction, for global-Y direction the maximum stiffness was 733186 kN/m.

4.1.5 Stiffness Irregularity

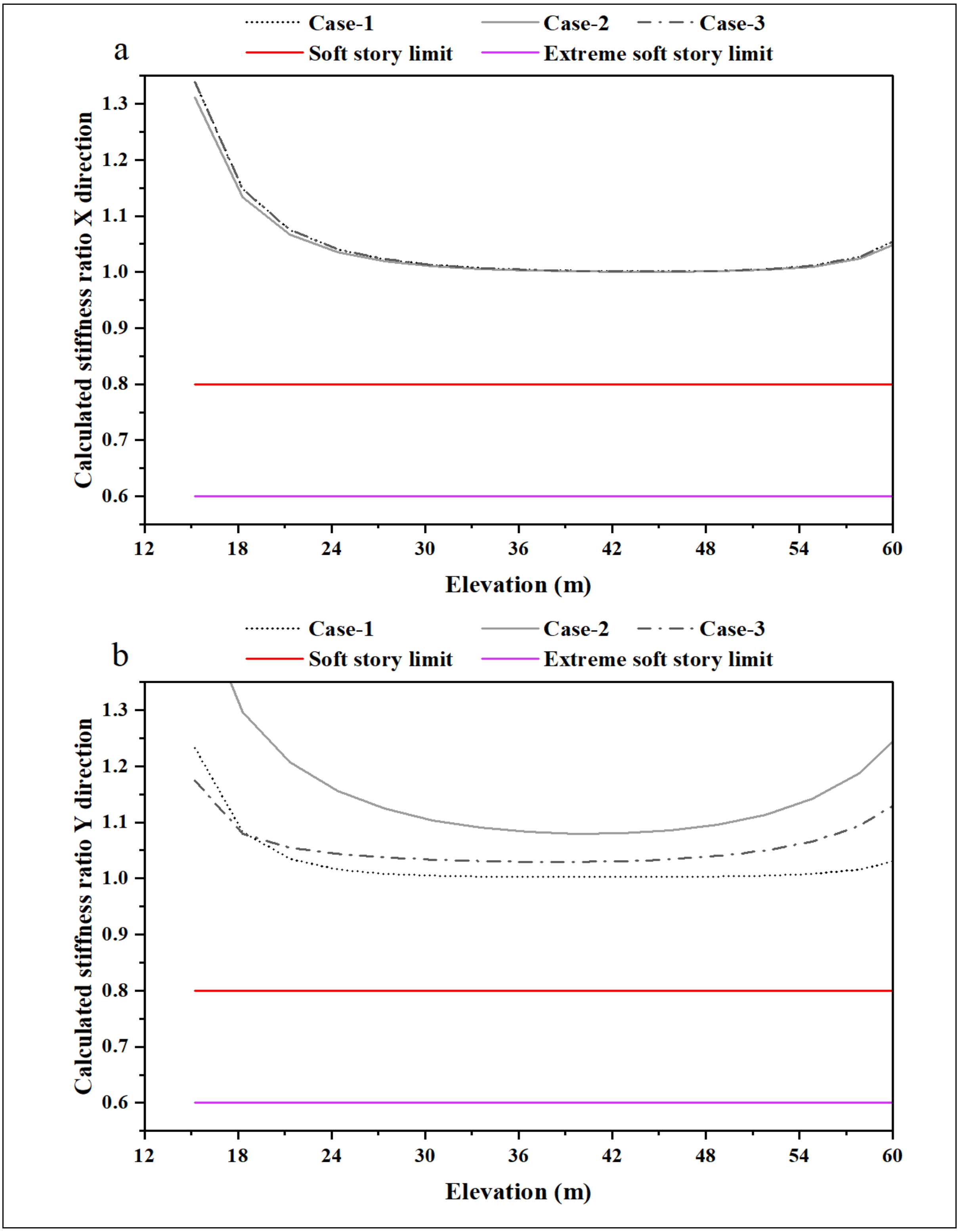

Figure 4.5: Story Stiffness at both Global X and Y Direction.

Figure 4.5 demonstrates the acceptable story stiffness ratios for each of the generated models. From the figure it can clearly be seen that bracing system and the shear wall played an important role to control the stiffness ratios in the global-X as well as the global-Y direction. Each of the models including Case-1 model which consisting only moment resisting frame was also able to control most of the stiffness ratio values under the allowable limit. The allowable stiffness was calculated from the guideline of ASCE 7-22, which is also presented in chapter 3. The obtained allowable drift ratio value was 0.8 for soft story and 0.6 for extreme soft story. For Case-1 model, the largest story stiffness ratio was found 1.33 and 1.23 while the lowest value was 1.001 and 1.002 at both X and Y direction respectively. As per the illustration of graphical representation, all of the story for Case-1 model passed according to the allowable limit.

Conversely, the maximum story stiffness ratio for Case-2 model was 1.31 and 1.50 while the minimum value was 1.006 and 1.07 at both X and Y direction respectively. Additionally, for Case-3 model, the maximum story stiffness ratio was 1.339 and 1.174 at both X and Y direction respectively. On the other hand, the minimum story stiffness ratio for Case-3 model was 1.009 and 1.029 at both X and Y direction respectively. Both Case-2 and Case-3 models consisting bracing and shear wall were able to keep the stiffness ratio value under the allowable limit.

4.1.6 Base Shear

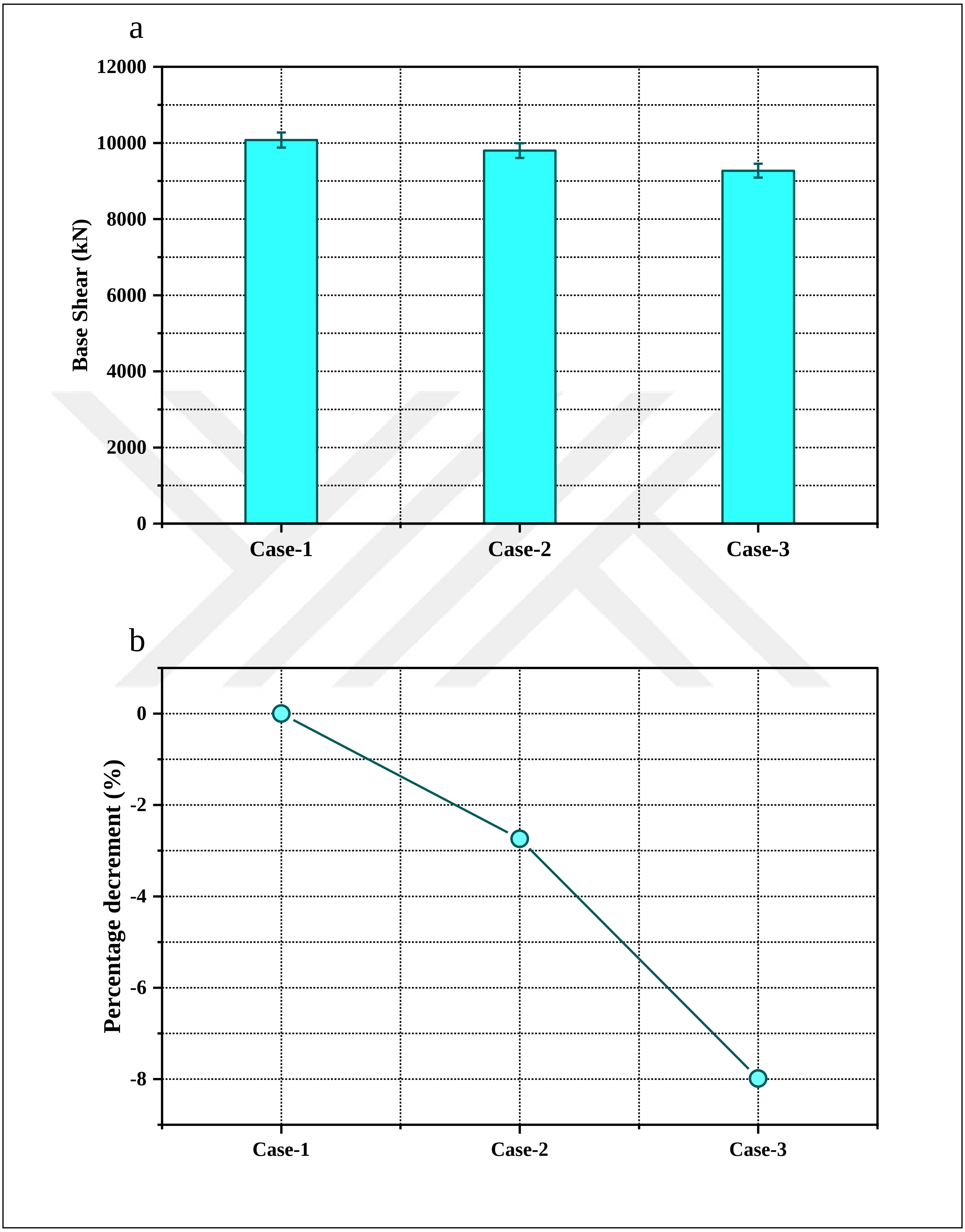

Figure 4.6: Base Shear Value and the % Change of Base Shear.

Figure 4.6 shows the base shear values for all models that have been constructed. From the dynamic analysis, it can be found that the model with bracing system depicted much better and for the Case-3, the base shear has been the minimum in the global-X as well as global-Y directions. The maximum base shear for this model was 9270 kN. On the other hand, Case-2 model consisting of shear wall at the core also depicted base shear of 9799 kN under the seismic load. This base shear value was 2.77% less than the Case-1 model which only consists of moment resisting frame. The Case-1, which only included MRF, displayed base shear that was approximately 8% greater than case-3's top-performing model. The base shear value for this model was 10075 kN. The model consisting only moment resisting frame depicted the highest base shear under the ground acceleration since it missed a stiffer structure to prevent earthquake loads.

4.1.7 Maximum Overturning Moment

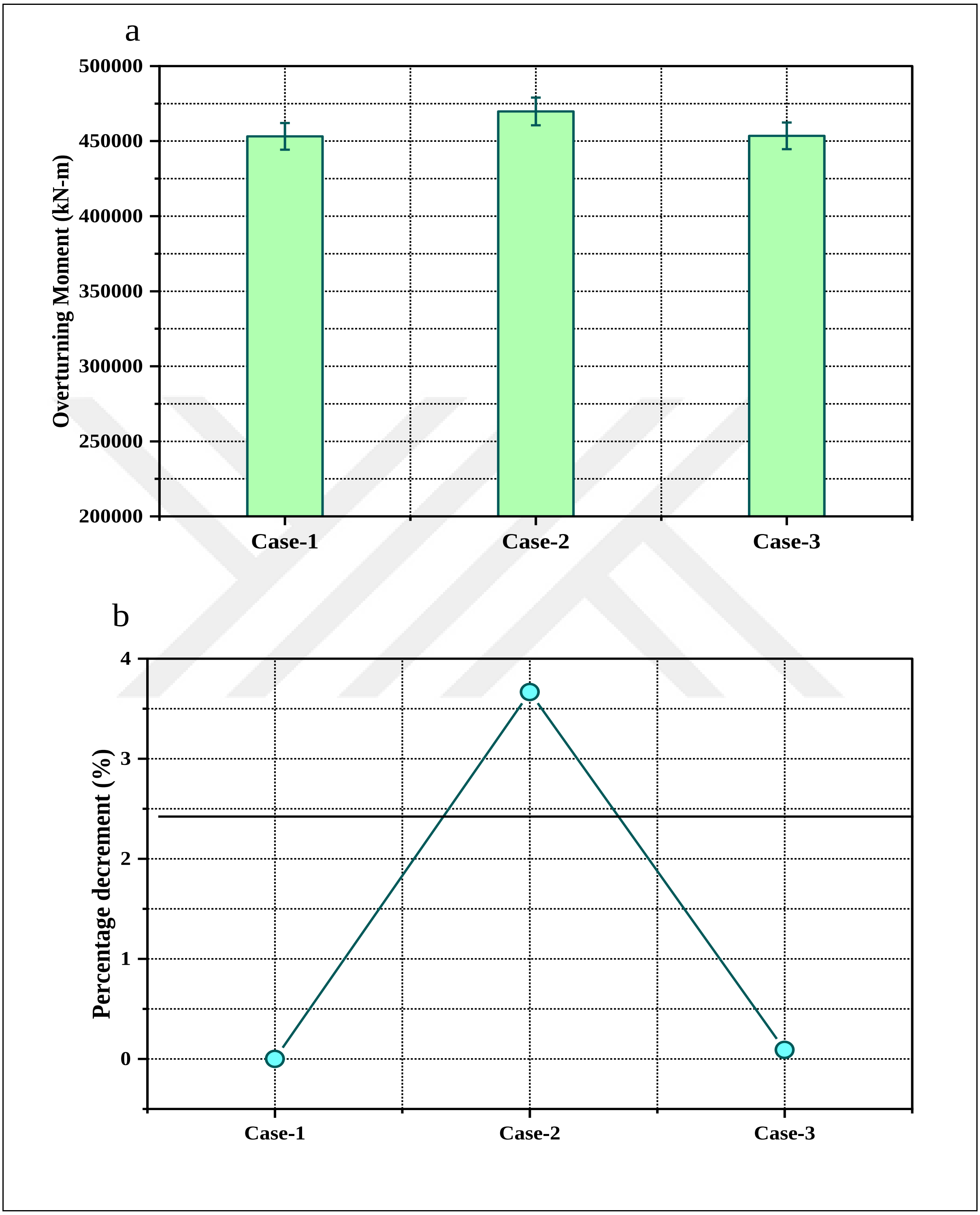

Figure 4.7: Maximum Overturning Moment Value and The % Change of the Value.

Figure 4.7 illustrates the results of maximum overturning moment for the developed models. From the dynamic analysis, it can be found that the model having bracing performed better; the maximum overturning moment was the lowest for this Case-3. The maximum overturning moment for this model was 443538 kN-m. On the other hand, Case-2 model consisting of shear wall at the core also depicted the maximum overturning moment which was 469746 kN-m under the seismic load. This maximum overturning moment value was 3.66% greater than the Case-1 model which only consists of moment resisting frame. The Case-1, which solely contained MRF, displayed a maximum average overturning moment that was 0.89% higher than the case-3's top-performing model. For this model, the highest overturning moment was 453132 kN-m. All the maximum overturning moment was obtained after the response spectrum analysis, with ensuring more that 90% model mass participation ratio.

4.1.8 Torsional Irregularity

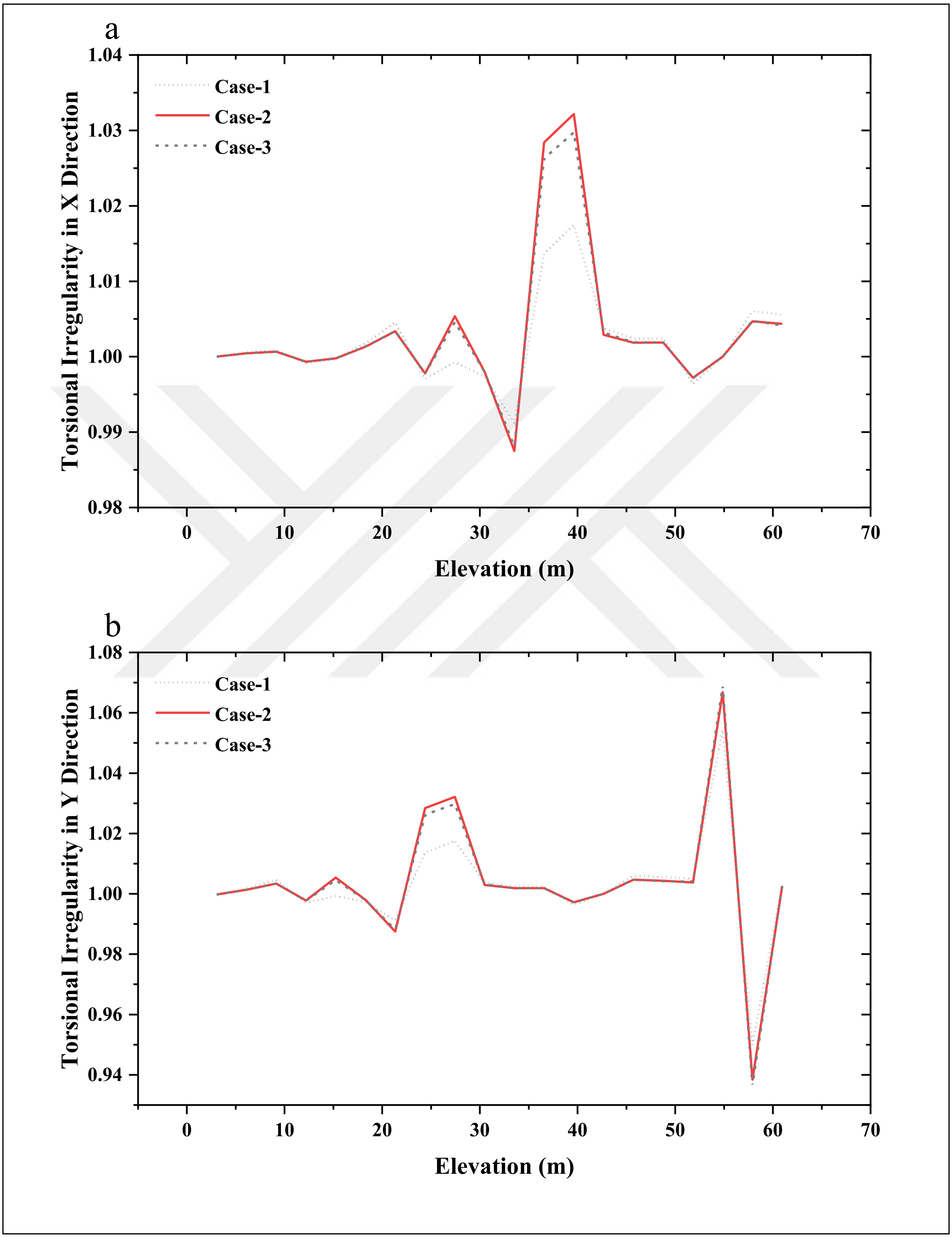

Figure 4.8: Story Mass-Weight Ratio (Torsional Irregularity) at both Global X and Y Direction.

Figure 4.8 depicts the story mass-weight ratio findings for all developed models. From the figure it can clearly be seen that bracing and the shear wall was crucial in controlling its entire story mass-weight ratio in the global-X as well as the global-Y direction. Every model including Case-1 model which consisting only moment resisting frame was also able to control the story torsional irregularity under the allowable limit. The allowable story mass-weight ratio for torsional irregularity was calculated from the guideline of ASCE 7-22, which is also presented in chapter 3. The obtained allowable story mass-weight ratio value was 1.2 for torsional irregularity and for extreme torsional irregularity, it was 1.4. For Case-1 model, the maximum story mass-weight ratio was 1.017 and 1.054 whereas the minimum story stiffness ratio was 0.99 and 0.942 at both the X and Y direction respectively. The graphical representation illustrates that all of the story for Case-1 model passed according to the allowable limit.

Conversely, the maximum mass-weight ratio for Case-2 model was 1.03 and 1.06 while the minimum value was 0.987 and 0.983 at both X and Y direction respectively. Additionally, the maximum value of the mass-weight ratio for Case-3 model was 1.029 and 1.068 at both X and Y direction respectively. On the other hand, the minimum mass-weight ratio for Case-3 model was 0.988 and 0.936 at both X and Y direction respectively.

4.1.9 Fundamental Time Period

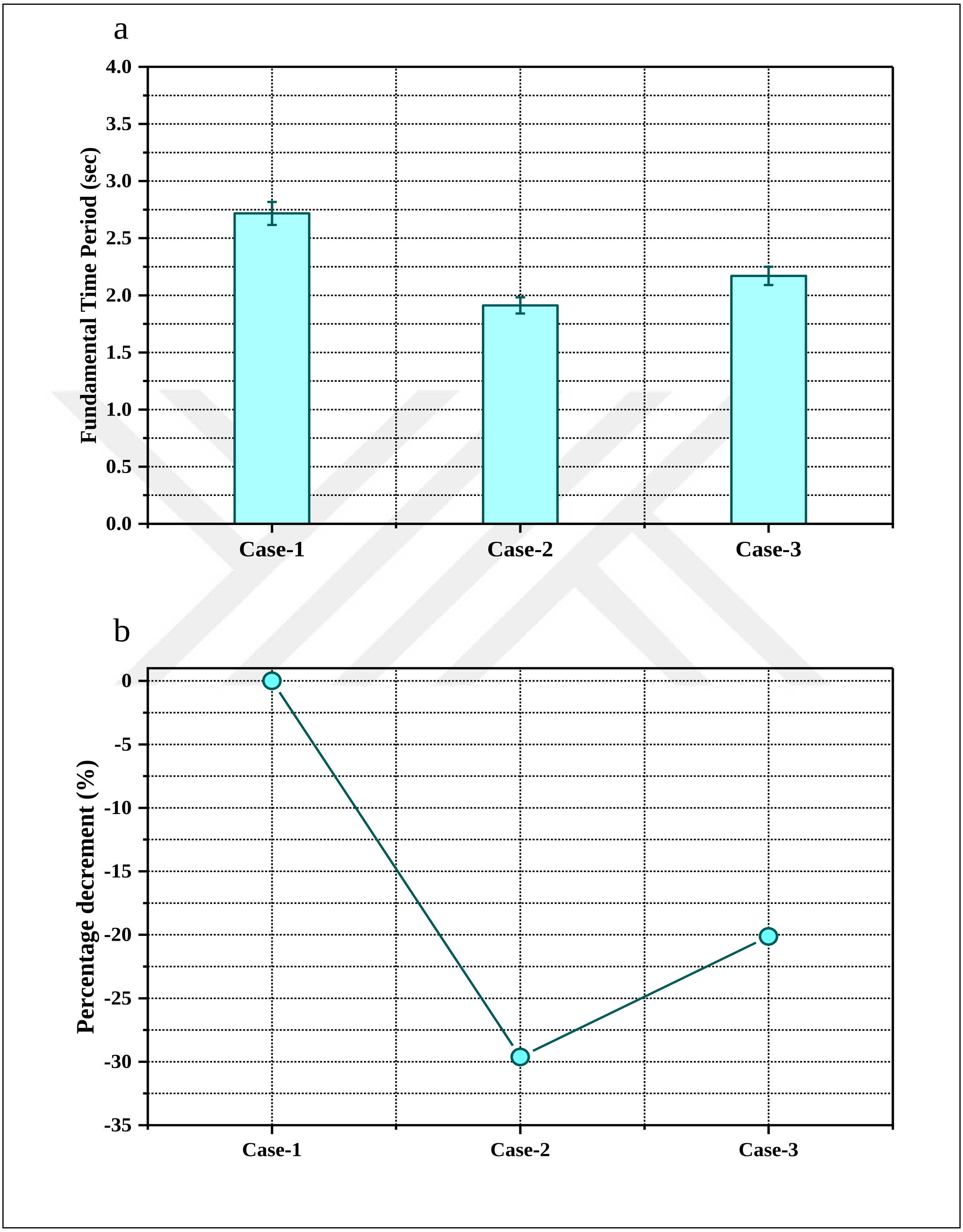

Figure 4.9: Fundamental Time Period Value and The % Change of Time Period.

Figure 4.9 illustrates the results of fundamental time period for the generated models. From the dynamic analysis, it can be observed that the model having shear wall at the core performed better; the fundamental time period was the lowest for this Case-2. The maximum fundamental time period for this model was 1.912 s. On the other hand, Case-3 model consisting of bracing also depicted fundamental time period of 2.17 s under the seismic load. This fundamental time period value was 20% less than the Case-1 model which only consists of moment resisting frame. The Case-1, which exclusively used MRF, displayed a fundamental time period that was 29.6% greater than the Case-2's top-performing model. The fundamental time period value for this model was 2.71 s. All the fundamental time period was obtained after the response spectrum analysis, with ensuring more that 90% model mass participation ratio.

4.2 RESULTS OF THE TIME HISTORY ANALYSIS

4.2.1 Base Shear

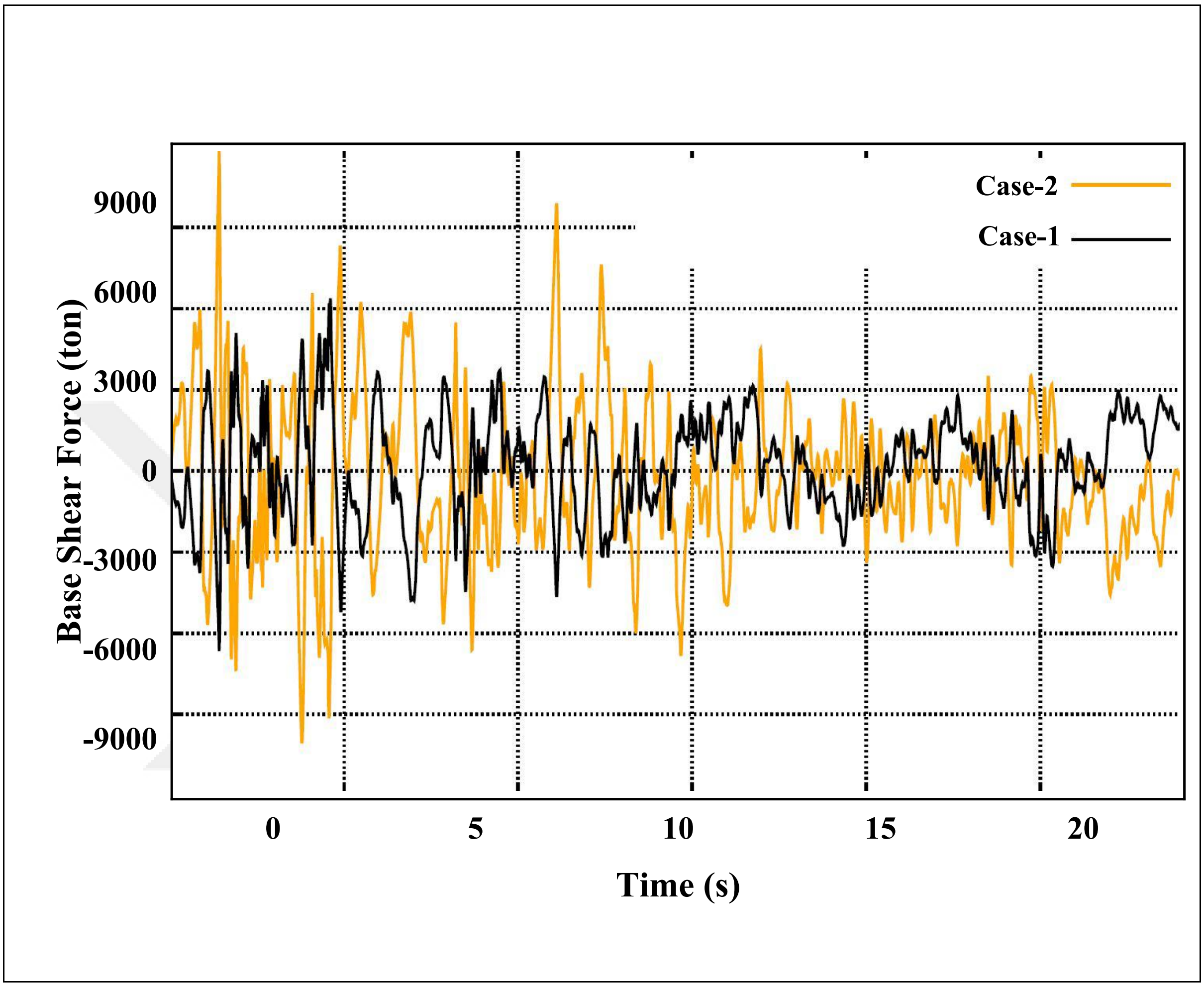

Figure 4.10: Joint Base Shear for THA.

Base shear stress is shown vs time in Figure 4.10. Incorporating a shear wall has resulted in a about 5.77 percent (Case-2) reduction in the stress at the bottom. As can be observed, the base shear force for such shear wall simulation has been reduced for a significant portion of the period, which demonstrates that the structure goes under a significant amount of stress when the earthquake is being excited. Therefore, this decrease in generated forces contributes to a minimization in the construction of the engineering structures, which in turn results in a considerable reduction in the overall weight of the structure, which in turn results in a lowering of the cost of building.

4.2.2 Energy Dissipation

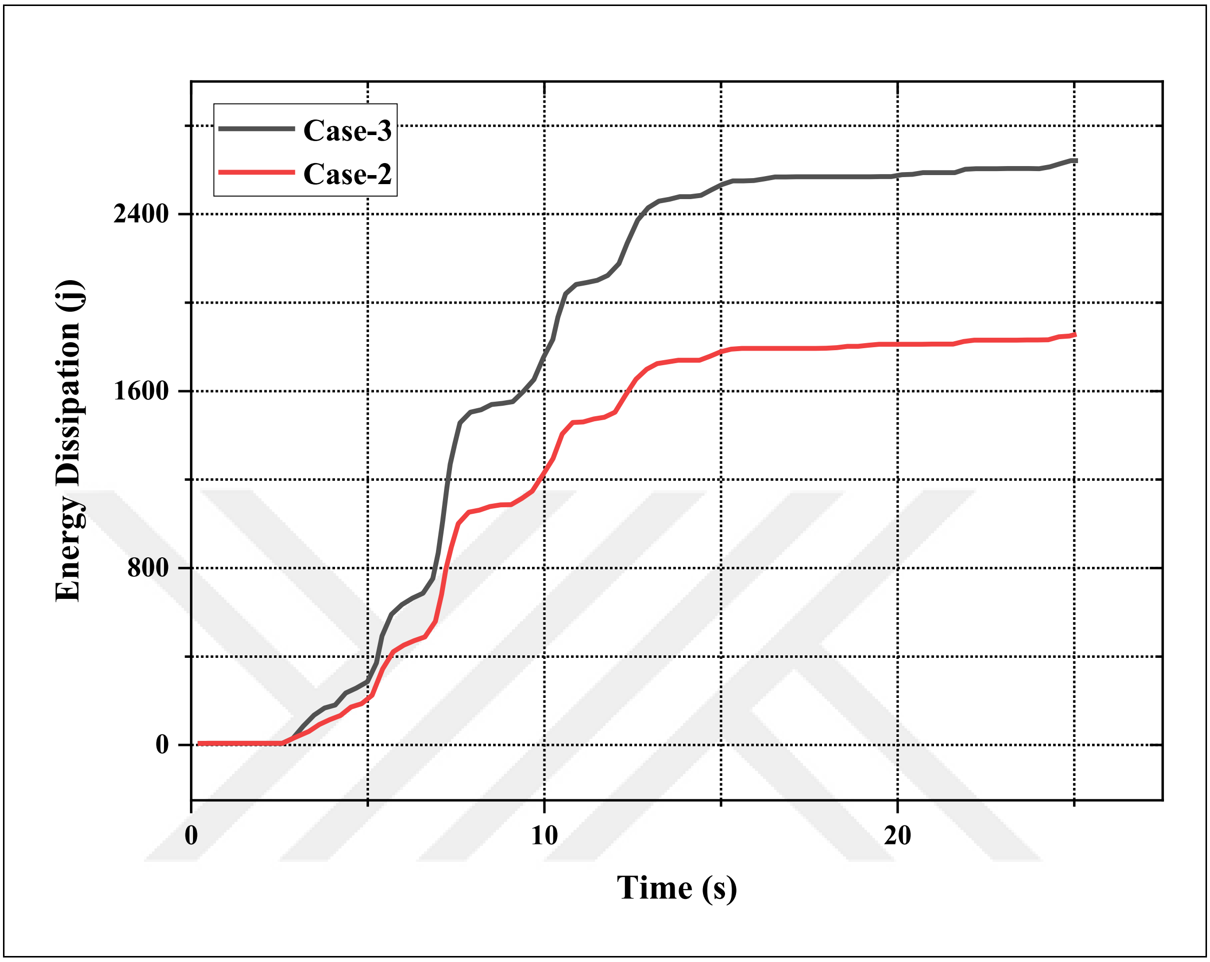

Figure 4.11: Energy Dissipation for both Case-2 and Case-3 Models.

The over-all energy dissipation for both the model consisting bracing system (Case-3) and Shear-wall at the core (Case-2) are depicted at Figure 4.11. From the analysis it can be seen that the maximum energy dissipation was observed for the bracing model in Case-3. The maximum energy dissipation was 2642.09 jule, while the minimum energy dissipation for this model was 6.18 jule. On the other hand the Case-2 model consisting of Shear-wall depicted great energy reduction performance against the EI-Centro earthquake. The maximum energy dissipation was 1857.8 jule, while the minimum energy dissipation for this model was 7.31 jule.

4.2.3 Absorbed Shear Percentage

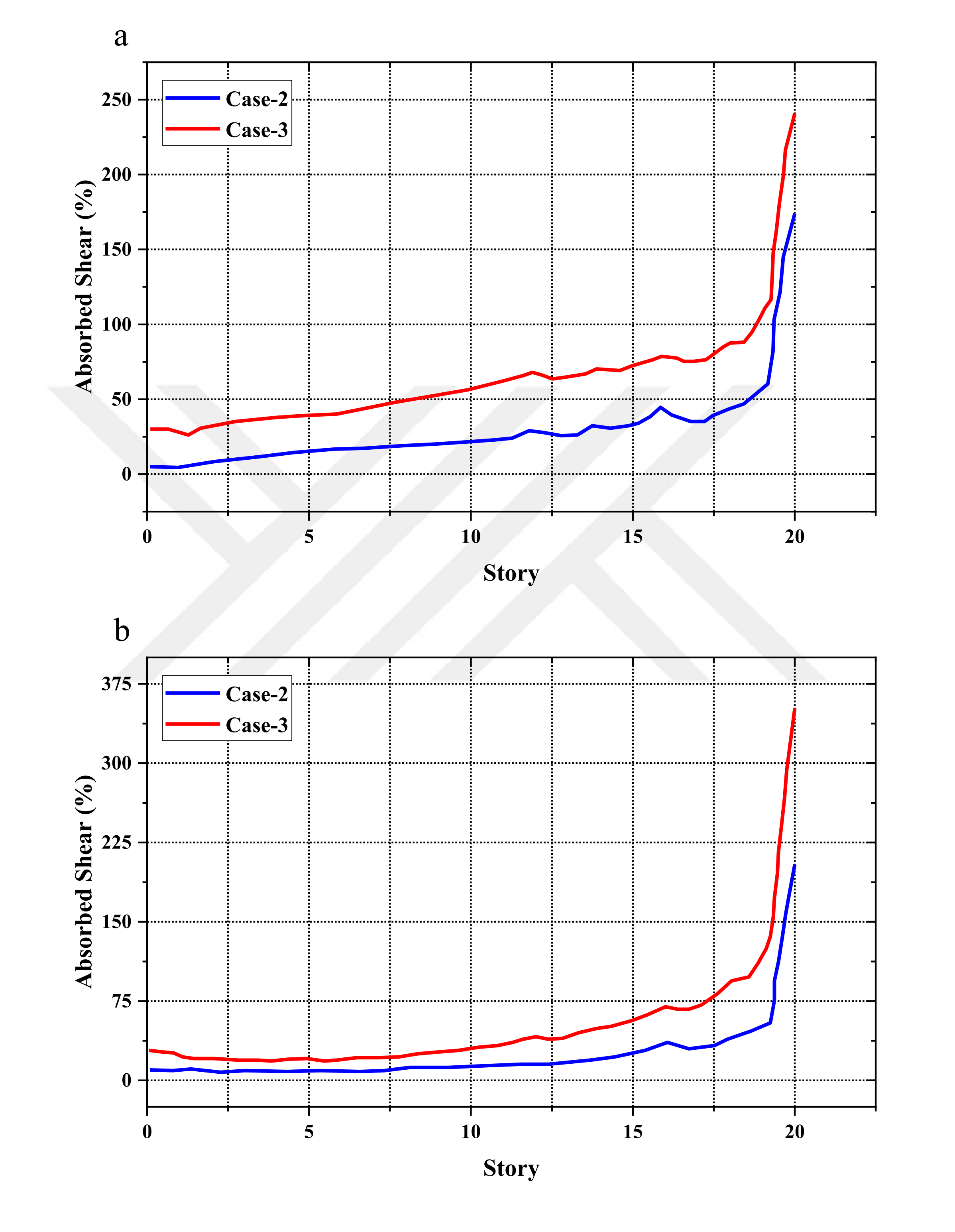

Figure 4.12: Absorbed Shear % at both Directions.

Figure 4.12 shows the absorbed shear percentage values for all models that have been constructed. Against the EI-Centro earthquake analysis it can be seen that bracing and the shear wall was crucial in controlling its entire story absorbed shear at both the directions. For Case-2 model, the maximum absorbed energy % was 173.97 and 204.20 whereas the minimum absorbed energy % was 4.46 and 26.20 at both the X and Y direction respectively.

Conversely, the maximum absorbed energy % for Case-3 model was 240.89 and 351.77 while the minimum value was 26.20 and 18.35 at both X and Y direction respectively.

4.2.4 Roof Displacement

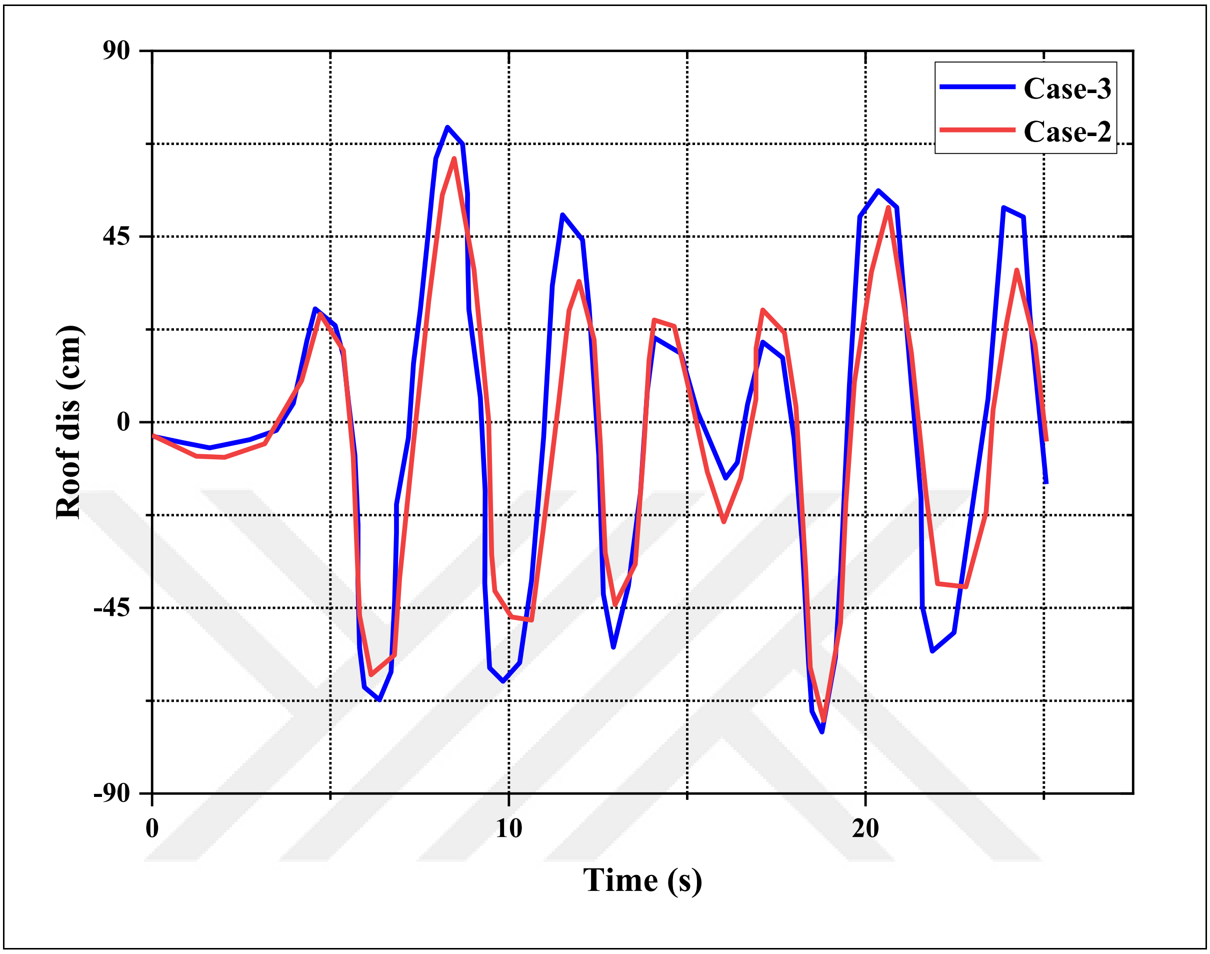

Figure 4.13: Roof Displacement.

The over-all roof displacement for both the model consisting bracing system (Case-3) and bracing system (Case-2) are depicted at Figure 4.13. From the analysis it can be seen that the maximum roof displacement was observed for the bracing model in Case-3. The maximum roof displacement was 71.48, while the minimum roof displacement for this model was 65.08. On the other hand, the Case-2 model consisting of Shear-wall depicted great roof displacement performance against the EI-Centro earthquake. The maximum roof displacement was 61.97, while the minimum roof displacement for this model was 52.

5. CONCLUSION

In view of the huge possibility for the deployment of current reliability systems in the structures, it is imperative that the efficiency of each method be evaluated, analyzed, and demonstrated in order to persuade the firms that design buildings to adopt them. Given this, the earthquake resistant standards that are used in modern times deliver a somewhat simplified model of a full view when it comes to evaluating the loads that are caused by seismic activity. This might or might not be directly proportionate with the comprehensive mathematical modelling effort that is frequently spent in portraying the structural system. Therefore, it was possible to compare the various structural systems in both linear dynamic and the time history scenarios in which substantial amounts of inelastic deformations are anticipated. The analysis yields the following conclusions:

a. It was found that by stiffening the high-rise structure with a structural model, the displacement and story drift during ground motion can be kept within limits.

b. Using both brace frames and shear wall at the core has a significant impact on control structure displacement, horizontal irregularities, and overturning moment over MRF model. To control the stiffness irregularity of the high-rise structural system. In terms of story displacement, the model consisting of shear wall at the core (Case-2) depicted 76% less story displacement than the MRF model (Case-1). Also the Case-2 model consisting core shear wall depicted 3% less base shear, while the Case-3 model depicted 8% less base shear than the Case-1 model.

c. Compared to the MRF theory, the model consisting of shear wall at the core (Case-2) depicted 26% less story drift than the MRF model (Case-1), while the Case-3 model depicted 15% less base shear than the Case-1 model.

d. Because of the regular rectangular form of the structures, no evidence of torsional irregularity could be seen in either the global-X or the global-Y direction.

e. In terms of fundamental period, the MRF theory, the model consisting of shear wall at the core (Case-3) depicted 30% less time period than the MRF model (Case-1), while the Case-3 model depicted 21% less than the Case-1 model.

f. From the data of the non-linear analysis the Case-2 model depicted 11.8% less roof displacement also the maximum energy dissipation was 39% less than the Case-3 model which consists of bracing frame

g. Absorbed shear was significantly less for the shear-wall system than the model consists of bracing system. Against the EI-Centro earthquake analysis it can be seen that bracing and the shear wall was crucial in controlling its entire story absorbed shear at both the directions. For Case-2 model, the maximum absorbed energy % was 173.97 and 204.20 whereas the minimum absorbed energy % was 4.46 and 26.20 at both the X and Y direction respectively. Conversely, the maximum absorbed energy % for Case-3 model was 240.89 and 351.77 while the minimum value was 26.20 and 18.35 at both X and Y direction respectively.

REFERENCES

[1] M. Erdik and N. Apaydın, "Earthquake response of suspension bridges," in *Vibration problems ICOVP 2005*, 2007, pp. 181-194: Springer.

[2] A. G. Sextos, K. D. Pitilakis, and A. J. Kappos, "Inelastic dynamic analysis of RC bridges accounting for spatial variability of ground motion, site effects and soil–structure interaction phenomena. Part 1: Methodology and analytical tools," *Earthquake engineering & structural dynamics,* vol. 32, no. 4, pp. 607-627, 2003.

[3] A. Kappos, *Dynamic loading and design of structures*. CRC Press, 2001.

[4] J. E. Padgett and R. DesRoches, "Sensitivity of seismic response and fragility to parameter uncertainty," *Journal of Structural Engineering,* vol. 133, no. 12, pp. 1710-1718, 2007.

[5] G. Mavroeidis, G. Dong, and A. Papageorgiou, "Near-fault ground motions, and the response of elastic and inelastic single-degree-of-freedom (SDOF) systems," *Earthquake Engineering & Structural Dynamics,* vol. 33, no. 9, pp. 1023-1049, 2004.

[6] G. D. Manolis, "Stochastic soil dynamics," *Soil Dynamics and Earthquake Engineering,* vol. 22, no. 1, pp. 3-15, 2002.

[7] E. Reis and D. Bonowitz, "State of the art report on past performance of steel moment-frame buildings in earthquakes," *SAC Rep. No. FEMA 355e, Federal Emergency Management Agency, Washington, DC,* 2000.

[8] M. Nakashima, K. Inoue, and M. Tada, "Classification of damage to steel buildings observed in the 1995 Hyogoken-Nanbu earthquake," *Engineering Structures,* vol. 20, no. 4-6, pp. 271-281, 1998.

[9] N. Luco and C. A. Cornell, "Effects of connection fractures on SMRF seismic drift demands," *Journal of Structural Engineering,* vol. 126, no. 1, pp. 127-136, 2000.

[10] B. F. Maison and K. Kasai, "Analysis of Northridge damaged thirteen-story WSMF building," *Earthquake spectra,* vol. 13, no. 3, pp. 451-473, 1997.

[11] D. Lignos, Y. Chung, T. Nagae, and M. Nakashima, "Numerical and experimental evaluation of seismic capacity of high-rise steel buildings subjected to long duration earthquakes," *Computers & Structures,* vol. 89, no. 11-12, pp. 959-967, 2011.

[12] K. Lee and D. A. Foutch, "Seismic performance evaluation of pre-Northridge steel frame buildings with brittle connections," *Journal of Structural Engineering,* vol. 128, no. 4, pp. 546-555, 2002.

[13] S. J. Venture and G. D. Committee, *Recommended seismic design criteria for new steel moment-frame buildings*. Federal Emergency Management Agency Washington, DC, USA, 2000.

[14] M. Nakashima, C. W. Roeder, and Y. Maruoka, "Steel moment frames for earthquakes in United States and Japan," *Journal of Structural Engineering,* vol. 126, no. 8, pp. 861-868, 2000.

[15] K. Hayashi and H. Inamasu, "Seismic performance of concrete-filled steel tube columns using ultra-high-strength steel under long-period ground motion demands," *Advances in Structural Engineering,* p. 13694332221145332, 2022.

[16] S. Nepal and M. Saitoh, "Improving the performance of conventional base isolation systems by an external variable negative stiffness device under near-fault and long-period ground motions," *Earthquake Engineering and Engineering Vibration,* vol. 19, pp. 985-1003, 2020.

[17] Y. L. Chung, T. Nagae, T. Matsumiya, and M. Nakashima, "Seismic resistance capacity of beam–column connections in high-rise buildings: E-Defense shaking table test," *Earthquake Engineering & Structural Dynamics,* vol. 40, no. 6, pp. 605-622, 2011.

[18] B. Stojadinovic, "Stability and low-cycle fatigue limits of moment connection rotation capacity," *Engineering structures*, vol. 25, no. 5, pp. 691-700, 2003.

[19] K. Mochizuki and K. Obana, "Seismic activities along the Nankai trough," *Bull. Earthq. Res. Inst,* vol. 78, pp. 185-195, 2003.

[20] K. Kamae, H. Kawabe, and K. Irikura, "Strong ground motion prediction for huge subduction earthquakes using a characterized source model and several simulation techniques," in *Proceedings of the 13th WCEE*, 2004.

[21] M. Saatcioglu *et al.*, "Performance of reinforced concrete buildings during the 27 February 2010 Maule (Chile) earthquake," *Canadian Journal of Civil Engineering,* vol. 40, no. 8, pp. 693-710, 2013.

[22] M. Sarrazin, O. Moroni, C. Neira, and B. Venegas, "Performance of bridges with seismic isolation bearings during the Maule earthquake, Chile," *Soil dynamics and earthquake engineering,* vol. 47, pp. 117-131, 2013.

[23] X. Ji, G. L. Fenves, K. Kajiwara, and M. Nakashima, "Seismic damage detection of a full-scale shaking table test structure," *Journal of Structural Engineering,* vol. 137, no. 1, pp. 14-21, 2011.

[24] K. Suita, Y. Kitamura, T. Goto, T. Iwata, and K. Kamae, "Seismic response of high-rise buildings constructed in 1970s subjected to long-period ground motions," *Journal of Structural and Construction Engineering,* vol. 611, pp. 55-61, 2007.

[25] M. Nakashima, T. Minami, and I. Mitani, "Moment redistribution caused by beam fracture in steel moment frames," *Journal of Structural Engineering,* vol. 126, no. 1, pp. 137-144, 2000.

[26] G. Abdollahzadeh, H. Faghihmaleki, and H. Esmaili, "Comparing Hysteretic Energy and inter-story drift in steel frames with V-shaped brace under near and far fault earthquakes," *Alexandria Engineering Journal,* vol. 57, no. 1, pp. 301-308, 2018.

[27] Z. Wen, Y. Hu, and K. T. Chau, "Site effect on vulnerability of high-rise shear wall buildings under near and far field earthquakes," *Soil Dynamics and Earthquake Engineering,* vol. 22, no. 9-12, pp. 1175-1182, 2002.

[28] V. Sharif and F. Behnamfar, "Evaluating the effects of near-field earthquakes on the behavior of moment resisting frames," *Computational Methods in Civil Engineering,* vol. 3, no. 2, pp. 79-91, 2012.

[29] E. Kalkan and S. K. Kunnath, "Effects of fling step and forward directivity on seismic response of buildings," *Earthquake spectra,* vol. 22, no. 2, pp. 367-390, 2006.

[30] A. Alonso-Rodríguez and E. Miranda, "Assessment of building behavior under near-fault pulse-like ground motions through simplified models," *Soil Dynamics and Earthquake Engineering,* vol. 79, pp. 47-58, 2015.

[31] M. Tehranizadeh and A. Meshkat-Dini, "Non-linear response of high rise buildings to pulse type strong ground motions," *Proceeding of the Australian Earthquake Engineering Society, Wollongong, Australia,* 2007.

[32] S. Goel, "Cyclic post buckling behavior of steel bracing members," *Stability and ductility of steel structures under cyclic loading,* pp. 75-104, 1992.

[33] X. Tang, *Seismic analysis and design considerations of braced steel structures*. University of Michigan, 1987.

[34] S. C. Goel and X. Tang, "Earthquake resistant design of ductile braced structures," ed: CRC press, 1992, pp. 297-308.

[35] D. J. Kelly, D. R. Bonneville, and S. J. Bartoletti, "1994 Northridge earthquake: damage to a four-story steel braced frame building and its subsequent upgrade," in *12th World Conference on Earthquake Engineering*, 2000.

[36] R. S. Olson, "The Political Economy Of Life-Safety: The City Of Los Angeles And “Hazardous-Structure Abatement,” 1973–1981," *Review of Policy Research,* vol. 4, no. 4, pp. 670-679, 1985.

[37] I. Gupta, "The state of the art in seismic hazard analysis," *ISET J Earthq Technol,* vol. 39, no. 4, pp. 311-346, 2002.

[38] E. L. Krinitzsky, "Deterministic versus probabilistic seismic hazard analysis for critical structures," *Engineering geology,* vol. 40, no. 1-2, pp. 1-7, 1995.

[39] R. Romeo and A. Prestininzi, "Probabilistic versus deterministic seismic hazard analysis: an integrated approach for siting problems," *Soil Dynamics and Earthquake Engineering,* vol. 20, no. 1-4, pp. 75-84, 2000.

[40] S. T. Algermissen, D. Perkins, P. Thenhaus, S. Hanson, and B. Bender, "Probabilistic estimates of maximum acceleration and velocity in rock in the contiguous United States," US Geological Survey2331-1258, 1982.

[41] L. Reiter, "Earthquake Hazard Analysis: Issues and Insights: New York," ed: Columbia, 1990.

[42] E. L. Krinitzsky, "The hazard in using probabilistic seismic hazard analysis for engineering," *Environmental & Engineering Geoscience,* vol. 4, no. 4, pp. 425-443, 1998.

[43] P. K. Malhotra, "Seismic risk and design loads," *Earthquake spectra,* vol. 22, no. 1, pp. 115-128, 2006.

[44] M. D. Trifunac, "Threshold magnitudes which cause the ground motion exceeding the values expected during the next 50 years in a metropolitan area," *Geofizika,* vol. 6, no. 1, pp. 1-12, 1989.

[45] R. K. McGuire, "Probabilistic seismic hazard analysis and design earthquakes: closing the loop," *Bulletin of the Seismological Society of America,* vol. 85, no. 5, pp. 1275-1284, 1995.

[46] P. Bazzurro and C. Allin Cornell, "Disaggregation of seismic hazard," *Bulletin of the Seismological Society of America,* vol. 89, no. 2, pp. 501-520, 1999.

[47] N. Haghi, S. Epackachi, and M. T. Kazemi, "Macro modeling of steel-concrete composite shear walls," in *Structures*, 2020, vol. 23, pp. 383-406: Elsevier.

[48] R. Rahnavard, A. Hassanipour, M. Suleiman, and A. J. J. o. B. E. Mokhtari, "Evaluation on eccentrically braced frame with single and double shear panels," vol. 10, pp. 13-25, 2017.

[49] M. Naghavi, R. Rahnavard, R. J. Thomas, and M. J. J. o. B. E. Malekinejad, "Numerical evaluation of the hysteretic behavior of concentrically braced frames and buckling restrained brace frame systems," vol. 22, pp. 415-428, 2019.

[50] R. Rahnavard, M. Naghavi, M. Aboudi, and M. J. C. S. i. C. M. Suleiman, "Investigating modeling approaches of buckling-restrained braces under cyclic loads," vol. 8, pp. 476-488, 2018.

[51] R. Rahnavard, A. Hassanipour, and A. J. J. o. C. S. R. Mounesi, "Numerical study on important parameters of composite steel-concrete shear walls," vol. 121, pp. 441-456, 2016.

[52] N. Haghi, S. Epackachi, and M. T. Kazemi, "Cyclic performance of composite shear walls with boundary elements," in *Structures*, 2020, vol. 27, pp. 102-117: Elsevier.

[53] B. Shafei, F. Zareian, and D. G. J. E. S. Lignos, "A simplified method for collapse capacity assessment of moment-resisting frame and shear wall structural systems," vol. 33, no. 4, pp. 1107-1116, 2011.

[54] S. Radkia, R. Rahnavard, H. Tuwair, F. A. Gandomkar, and R. Napolitano, "Investigating the effects of seismic isolators on steel asymmetric structures considering soil-structure interaction," in *Structures*, 2020, vol. 27, pp. 1029-1040: Elsevier.

[55] S. Etedali, K. Hasankhoie, and M. R. J. J. o. B. E. Sohrabi, "Seismic responses and energy dissipation of pure-friction and resilient-friction base-isolated structures: A parametric study," vol. 29, p. 101194, 2020.

[56] A. Lanzi and J. E. J. J. o. S. E. Luco, "Elastic velocity damping model for inelastic structures," vol. 144, no. 6, p. 04018065, 2018.

[57] C.-S. Tsai, Y.-M. Wang, and H.-C. J. I. J. o. O. I. Su, "SOIL-STRUCTURE INTERACTION, DAMPING AND HIGHER MODE EFFECTS ON THE RESPONSE OF A MID-STORY-ISOLATED STRUCTURE FOUNDED ON MULTIPLE SOIL LAYERS," vol. 1, no. 3, 2019.

[58] C. Adam, L. F. Ibarra, and H. Krawinkler, "Evaluation of P-delta effects in non-deteriorating MDOF structures from equivalent SDOF systems," 2004.

[59] E. Miranda and S. D. J. J. o. S. E. Akkar, "Dynamic instability of simple structural systems," vol. 129, no. 12, pp. 1722-1726, 2003.

[60] E. B. J. J. o. S. E. Williamson, "Evaluation of damage and P-Δ effects for systems under earthquake excitation," vol. 129, no. 8, pp. 1036-1046, 2003.

[61] H. Takizawa, P. C. J. E. E. Jennings, and S. Dynamics, "Collapse of a model for ductile reinforced concrete frames under extreme earthquake motions," vol. 8, no. 2, pp. 117-144, 1980.

[62] F. Zareian, H. Krawinkler, L. Ibarra, D. J. T. S. D. o. T. Lignos, and S. Buildings, "Basic concepts and performance measures in prediction of collapse of buildings under earthquake ground motions," vol. 19, no. 1-2, pp. 167-181, 2010.

[63] R. A. Medina, R. Sankaranarayanan, and K. M. J. E. s. Kingston, "Floor response spectra for light components mounted on regular moment-resisting frame structures," vol. 28, no. 14, pp. 1927-1940, 2006.

[64] D. Vamvatsikos and C. A. Cornell, "The incremental dynamic analysis and its application to performance-based earthquake engineering," in *Proceedings of the 12th European conference on earthquake engineering*, 2002, vol. 40: Citeseer.

[65] F. Zareian, H. J. E. E. Krawinkler, and S. Dynamics, "Assessment of probability of collapse and design for collapse safety," vol. 36, no. 13, pp. 1901-1914, 2007.

[66] S. A. Ahamad and K. J. M. T. P. Pratap, "Dynamic analysis of G+ 20 multi storied building by using shear walls in various locations for different seismic zones by using Etabs," 2020.

[67] J. Ji, A. S. Elnashai, and D. Kuchma, "Seismic fragility assessment for reinforced concrete high-rise buildings," *MAE Center CD Release 07-14*, 2007.

[68] W. Alwaeli, A. Mwafy, K. Pilakoutas, and M. Guadagnini, "Framework for developing fragility relations of high-rise RC wall buildings based on verified modelling approach," in *The Proceedings of the Second European Conference on Earthquake Engineering and Seismology*, 2014.

[69] Z. T. Değer, T. Y. Yang, J. W. Wallace, and J. Moehle, "Seismic performance of reinforced concrete core wall buildings with and without moment resisting frames," *The Structural Design of Tall and Special Buildings,* vol. 24, no. 7, pp. 477-490, 2015.

[70] Z. T. Değer and J. W. Wallace, "Seismic performance of reinforced concrete dual-system buildings designed using two different design methods," *The structural design of tall and special buildings,* vol. 25, no. 1, pp. 45-59, 2016.

[71] M. Aman, H. Nadeem, and E. S. Khaled, "Seismic performance and cost-effectiveness of high-rise buildings with increasing concrete strength," *The Structural Design of Tall and Special Buildings,* vol. 24, no. 4, pp. 257-279, 2015.

[72] E. S. Firoozabad, K. R. M. Rao, and B. Bagheri, "Effect of shear wall configuration on seismic performance of building," in *International Conference on Advances in Civil Engineering*, 2012, pp. 121-125: Citeseer.

[73] A. Chandiwala, "Earthquake analysis of building configuration with different position of shear wall," *International Journal of Emerging Technology and Advanced Engineering,* vol. 2, no. 12, pp. 347-353, 2012.

[74] S. J. Sardar and U. N. Karadi, "Effect of change in shear wall location on storey drift of multi Storey building subjected to lateral loads," *International Journal of Innovative Research in Science Engineering and Technology,* vol. 2, no. 9, 2013.

[75] J. Kim, J. Lee, and S. Han, "Seismic performance of building structures with spatial variability," *International Journal of Engineering and Technology,* vol. 5, no. 6, p. 721, 2013.

[76] T. Kagawa, K. Irikura, and P. G. Somerville, "Differences in ground motion and fault rupture process between the surface and buried rupture earthquakes," *Earth, Planets and Space,* vol. 56, pp. 3-14, 2004.

[77] A. S. Papageorgiou and K. Aki, "A specific barrier model for the quantitative description of inhomogeneous faulting and the prediction of strong ground motion.

Part II. Applications of the model," *Bulletin of the Seismological Society of America,* vol. 73, no. 4, pp. 953-978, 1983.

[78] B. Bolt, "Estimation of strong seismic ground motions," *International handbook of earthquake and engineering seismology,* pp. 983-1001, 2002.

[79] P.-S. Lin and C.-T. Lee, "Ground-motion attenuation relationships for subduction-zone earthquakes in northeastern Taiwan," *Bulletin of the Seismological Society of America,* vol. 98, no. 1, pp. 220-240, 2008.

[80] A. Kappos and P. Kyriakakis, "A re-evaluation of scaling techniques for natural records," *Soil Dynamics and Earthquake Engineering,* vol. 20, no. 1-4, pp. 111-123, 2000.

[81] E. I. Katsanos, A. G. Sextos, and G. D. Manolis, "Selection of earthquake ground motion records: A state-of-the-art review from a structural engineering perspective," *Soil dynamics and earthquake engineering,* vol. 30, no. 4, pp. 157-169, 2010.

[82] G. M. Atkinson and D. M. Boore, *Boore-Atkinson NGA ground motion relations for the geometric mean horizontal component of peak and spectral ground motion parameters*. Pacific Earthquake Engineering Research Center, 2007.

[83] P. J. Stafford, F. O. Strasser, and J. J. Bommer, "An evaluation of the applicability of the NGA models to ground-motion prediction in the Euro-Mediterranean region," *Bulletin of earthquake Engineering,* vol. 6, pp. 149-177, 2008.

[84] S. E. Abdel Raheem, "Evaluation of Egyptian code provisions for seismic design of moment-resisting-frame multi-story buildings," *International Journal of Advanced Structural Engineering,* vol. 5, no. 1, pp. 1-18, 2013.

[85] S. Mahmoud and W. Abdallah, "Response analysis of multi-Storey RC buildings under Equivalent static and dynamic loads according to Egyptian code," *International Journal of Civil and Structural Engineering Research,* vol. 2, no. 1, pp. 79-88, 2014.

[86] R. W. Clough and J. Penzien, "Dynamics of structures. Berkeley," *CA: Computers and Structures*, 2003.

[87] C.-C. Chen and A. Robinson, "Improved time-history analysis for structural dynamics. I: Treatment of rapid variation of excitation and material nonlinearity," *Journal of Engineering Mechanics,* vol. 119, no. 12, pp. 2496-2513, 1993.

[88] X. Chen and S. Mahmoud, "Implicit Runge–Kutta methods for Lipschitz continuous ordinary differential equations," *SIAM Journal on Numerical Analysis,* vol. 46, no. 3, pp. 1266-1280, 2008.

[89] S. Mahmoud and X. Chen, "A verified inexact implicit Runge–Kutta method for nonsmooth ODEs," *Numerical Algorithms,* vol. 47, no. 3, pp. 275-290, 2008.

[90] G. M. Atkinson and I. A. Beresnev, "Compatible ground-motion time histories for new national seismic hazard maps," *Canadian Journal of Civil Engineering,* vol. 25, no. 2, pp. 305-318, 1998.

[91] M. D. Trifunac, "Uniformly processed strong earthquake ground accelerations in the Western United States of America for the period from 1933-1971: pseudo relative velocity spectra and processing noise," 1977.

[92] A. K. Chopra, *Dynamics of structures*. Pearson Education India, 2007.

[93] P. K. Malhotra, "Response of buildings to near-field pulse-like ground motions," *Earthquake engineering & structural dynamics,* vol. 28, no. 11, pp. 1309-1326, 1999.

[94] F. Mollaioli, S. Bruno, L. D. Decanini, and G. F. Panza, "Characterization of the dynamic response of structures to damaging pulse-type near-fault ground motions," *Meccanica,* vol. 41, no. 1, pp. 23-46, 2006.

[95] A. Moustafa and I. Takewaki, "Characterization of earthquake ground motion of multiple sequences," *Earthquakes and Structures,* vol. 3, no. 5, pp. 629-647, 2012.

[96] ASCE-7-22, "Minimum Design Loads and Associated Criteria for Buildings and Other Structures," *American Society of Civil Engineers: Reston, VA, USA, 2022.,* 2022.

[97] S. A. Ahamad and K. Pratap, "Dynamic analysis of G+ 20 multi storied building by using shear walls in various locations for different seismic zones by using Etabs," *Materials Today: Proceedings,* vol. 43, pp. 1043-1048, 2021.

[98] S. Bharti, S. Dumne, and M. Shrimali, "Seismic response analysis of adjacent buildings connected with MR dampers," *Engineering Structures,* vol. 32, no. 8, pp. 2122-2133, 2010.